REPORT DOCUMENTATION PAGE

Form Approved
OMB No. 0704-0188

PLEASE DO NOT RETURN YOUR FORM TO THE ABOVE ORGANIZATION.

1. REPORT DATE *(DD-MM-YYYY)*	2. REPORT TYPE	3. DATES COVERED *(From - To)*
01-6-2012	Master's Thesis	JAN 2012 - JUN 2012

4. TITLE AND SUBTITLE
Design of a Free-running, 1/30th Froude Scaled Model Destroyer for In-situ Hydrodynamic Flow Visualization

5a. CONTRACT NUMBER
N00244-09-G-0014

5b. GRANT NUMBER

5c. PROGRAM ELEMENT NUMBER

6. AUTHOR(S)
David M. Cope

5d. PROJECT NUMBER

5e. TASK NUMBER

5f. WORK UNIT NUMBER

7. PERFORMING ORGANIZATION NAME(S) AND ADDRESS(ES)
Massachusetts Institute of Technology

8. PERFORMING ORGANIZATION REPORT NUMBER

9. SPONSORING/MONITORING AGENCY NAME(S) AND ADDRESS(ES)
Naval Postgraduate School
Monterey, CA 93943

10. SPONSOR/MONITOR'S ACRONYM(S)
NPS

11. SPONSOR/MONITOR'S REPORT NUMBER(S)

12. DISTRIBUTION/AVAILABILITY STATEMENT
1. DISTRIBUTION STATEMENT A. Approved for public release; distribution is unlimited.

13. SUPPLEMENTARY NOTES

14. ABSTRACT
Hydrodynamic flow visualization techniques of scaled hull forms and propellers are typically limited to isolating certain operating conditions in a tow tank, circulation tunnel, or large maneuvering basin. Although cost effective, these tests provide a limited perspective on the interactions of the entire system. Full-scale testing, other the other hand, provides real world data but is costly. In between, a Froude scaled, free-running model of an existing hull form controls costs but also provides superior hydrodynamic data that can be translated more accurately to full scale. This thesis details the design and construction of a 1/30th scale free-running model of the David Taylor Model Basin 5415 hull, the precursor to the ubiquitous Arleigh Burke Guided Missile Destroyer hull. The model serves as an experimental platform for advanced maneuvering and propeller crashback studies.

15. SUBJECT TERMS

16. SECURITY CLASSIFICATION OF:			17. LIMITATION OF ABSTRACT	18. NUMBER OF PAGES	19a. NAME OF RESPONSIBLE PERSON
a. REPORT	b. ABSTRACT	c. THIS PAGE	UU	99	Julie Zack
					19b. TELEPHONE NUMBER *(Include area code)* (831) 656-2319

Reset

Design of a Free-running, 1/30th Froude Scaled Model Destroyer for In-situ Hydrodynamic Flow Visualization

By

David M. Cope, LT USN

Bachelor of Science in Ocean Engineering
United States Naval Academy, 2007

Submitted to the Department of Mechanical Engineering
In partial fulfillment of the requirements for the degrees of

Naval Engineer
and
Master of Science in Mechanical Engineering
at the
MASSACHUSETTS INSTITUTE OF TECHNOLOGY

June 2012

Signature of Author……

MIT Sea Grant
Naval Construction and Engineering Program (Course 2N)
May 11, 2012

Certified by……

Chryssostomos Chryssostomidis
Doherty Professor of Ocean Science and Engineering
Director, MIT Sea Grant College Program
Thesis Supervisor

Accepted by……...

Professor David E. Hardt
Chairman, Departmental Committee on Graduate Students
Department of Mechanical Engineering

(This Page Intentionally Left Blank)

Design of a Free-running, 1/30th Froude Scaled Model Destroyer for In-situ Hydrodynamic Flow Visualization

By

David M. Cope, LT USN

Submitted to the Department of Mechanical Engineering
On May 11, 2012, in Partial Fulfillment of the Requirements for the Degrees of

Naval Engineer

and

Master of Science in Mechanical Engineering

ABSTRACT

Hydrodynamic flow visualization techniques of scaled hull forms and propellers are typically limited to isolating certain operating conditions in a tow tank, circulation tunnel, or large maneuvering basin. Although cost effective, these tests provide a limited perspective on the interactions of the entire system. Full-scale testing, other the other hand, provides real world data but is costly. In between, a Froude scaled, free-running model of an existing hull form controls costs but also provides superior hydrodynamic data that can be translated more accurately to full scale. This thesis details the design and construction of a $1/30^{th}$ scale free-running model of the David Taylor Model Basin 5415 hull, the precursor to the ubiquitous Arleigh Burke Guided Missile Destroyer hull. The model serves as an experimental platform for advanced maneuvering and propeller crashback studies.

The propeller crashback (a core propulsion plant test for both the U.S. Navy and commercial vessels) imparts significant unsteady loads to the engineering plant and drive train. Each of these is respectively of interest to propeller designers and the Electric Ship Research and Development Consortium (ESRDC). The $1/30^{th}$ scale model provides unsteady, time-resolved, accurate 3D flow visualization and propeller loading data as well as measurements of the effects on the electrical propulsion motors. Testing conducted with the model provides the real world effects of the propeller flow interaction with the hull and appendages.

The second area of research concerns the high inefficiencies of slender hull forms while maneuvering. During a turn, a significant amount of power is lost to the low pressure region

developed on the inside of the turn from shedding vortices that originate along the keel. This increases the tactical diameter of the turn and reduces the turning efficiency of the vessel. Research is currently being conducted around controlling the shedding of vortices and keeping them attached to the hull thereby increasing the turning efficiency and decreasing the turning radius of the vessel. The final area of interest is in forward mounted podded propulsors for use on large vessels.

Thesis Supervisor: Chryssostomos Chryssostomidis
Title: Doherty Professor of Ocean Science and Engineering
Director, MIT Sea Grant College Program

ACKNOWLEDGEMENTS

Although it may appear that the design and construction of this model was the work of one person, nothing could be further from the truth. I am in great debt to a number of persons in academia, industry and the Navy. First and foremost, Professor Chryssostomos Chryssostomidis who provided the initial design concept and funded the construction of the model. Dr. Brenden Epps' patience, expertise, and mentoring in no small part kept the project on track and moving forward. Mike Soroka's vast knowledge of all things engineering and fabrication as well as his dedication to the project was an invaluable asset. Mark Belanger of the Edgerton Student Shop taught me the machining skills necessary to construct several components of the model. The engineers at Marine Applied Physics Corporation, Paul Dillingham and Kyle Moseson, who took my initial design and built a spectacular model and handled the design alterations with ease, are much appreciated. Mark Lamattina and Craig Deady, respectively of Target Electronic Supply and Kaman, lent me their time and knowledge on countless occasions to get the model control system and motors operating. When the size of the model grew too large to manage at Sea Grant's MIT lab, we went into a scramble trying to locate a lab space to house the model and complete the assembly. Fortunately, the generous people at Bluefin Robotics (Quincy, MA) again reaffirmed the close relationship between themselves and MIT Sea Grant and provided a first class facility to complete the project. Specifically, Will O'Halloran and Harvey Duplantis provided unyielding support at a moment's notice, without which the project would not have reached its current state.

Table of Contents

List of Figures

List of Tables

1 INTRODUCTION

1.1 Background and Overview

1.1.1 The Crashback Maneuver and Current Extent of Research

Large commercial and naval vessels alike constantly operate in congested sea lanes both on the open ocean and along the land-sea interface. In extreme circumstances, it is necessary to bring these several thousand ton vessels to an immediate stop to avoid collision or grounding. To achieve this maneuver, deck officers execute what is called the crashback maneuver, throwing the propulsion train into full reverse while operating at high ahead speeds. From the propeller's point of view, this maneuver is characterized by the forward inflow from the ahead motion of the ship while the propeller operates in reverse. If outfitted with a fixed pitch propeller, the entire drive train must decelerate to zero speed and accelerate in the astern direction, making the propeller's designed trailing edge the new leading edge. With controllable pitch propellers, the drive train maintains its ahead speed and the blades of the propeller mechanically rotate their pitch angle at the hub, effectively changing the inflow angle and reversing the direction of thrust. In both instances, the severity of the maneuver imparts extreme loads on both the propeller and drive train and has led to blade failure and damage to the shafting, reduction gears and main engines. The interaction of the opposing flows and resulting unsteadiness makes the crashback condition particularly difficult to analyze. Figure 1 depicts the dominant flow streamlines during the crashback event.

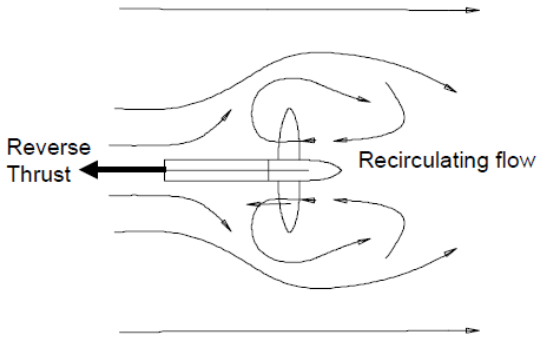

FIGURE 1-CRASHBACK FLOW CONDITION (REPRODUCED FROM [1])

Because of the potential for failure, the U.S. Navy includes this extreme off-design condition as a standard test of the engineering plant during delivery of a new ship and regularly throughout the life of the ship. Most of the propellers in the Navy's inventory are highly skewed and are more susceptible to blade failure from extreme loading. The leading ship engineering and research arm of the Navy, Naval Surface Warfare Division Carderock (NSWC-CD), has conducted extensive testing and research around the maneuver at both model and full scale. The core of the research has been conducted in recirculating water tunnels measuring blade stress and imaging the flow around the propeller through particle image velocimetry (PIV) or laser doppler velocimetry (LDV). Jessup et al. (2008) conducted a thorough examination of flow velocities around propeller 4381 at two advance coefficients, J=-0.5 and -0.7, in NSWC-CD's 36 inch water tunnel. The imaging was done in the X-R plane. Time averaged results show the distinctive vortex ring around the blade tip, caused by the downstream (astern) flow from the moving ship and the reverse flow through the propeller disk. As would be expected, the vortex ring shifts aft and expands as the free stream velocity increases (more negative J). Figure 2 shows the time averaged vortex ring around the blade tip.

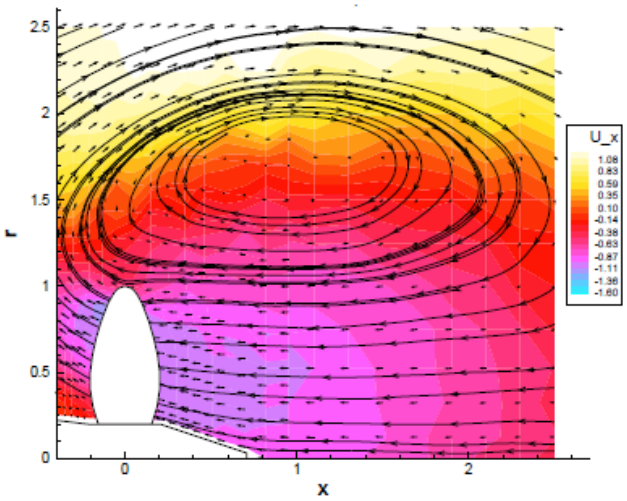

FIGURE 2-TIME AVERAGED AXIAL VELOCITY STREAMLINES FROM LDV AT J=-0.7 (REPRODUCED FROM [2])

Also witnessed during the course of the research was a diffuse blade wake which Jessup (2008) attributed to the unsteadiness of the blade flow during crashback event. This time-averaged velocity data was then utilized to calculate the mean blade stresses on each blade using existing potential flow based panel codes. The results showed increased suction along the

trailing edge because of flow separation. Jessup (2004) also notes that the standard geometric angle of attack when considering the 2D flow diagrams does not accurately represent the actual inflow and over predicts the angles of attack. As is seen in Figure 3, the net axial inflow to the blade sections is governed by the suction of the propeller and not the astern flow from the ship [2]. Figure 3shows the blade section inflow vectors where α is the angle of attack and Φ is the local pitch angle.

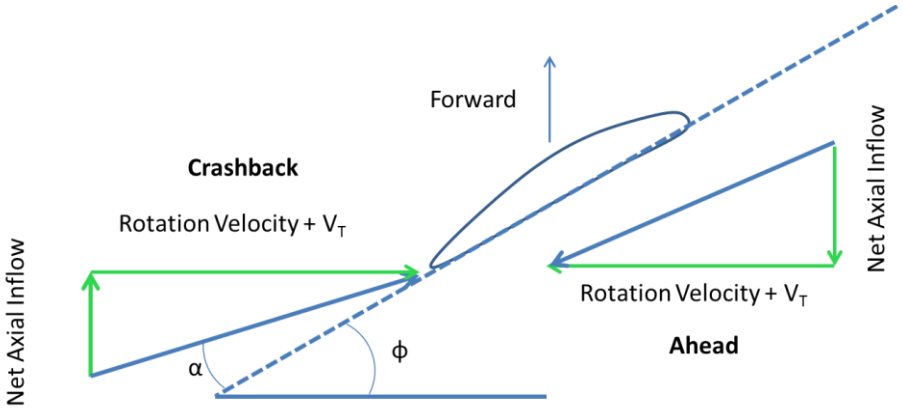

FIGURE 3-SECTIONAL BLADE INFLOW VECTORS

Of more interest than the average flow is fully time-resolved flow because of the large amount of unsteadiness around the propeller during crashback. The unsteadiness is seen in the sporadic inboard and outboard movement of the vortex ring and causes large fluctuations in thrust and torque on the propeller and drive train. PIV shows that the vortex moves from a time averaged location of 1.7 radii outboard to well inboard of the blade tip. The NSWC-CD research found that when the ring vortex moves inboard, towards the hub, the local axial flow at the blade tip is reversed from the time averaged axial flow. This drastically shifts the local angle of attack and was hypothesized to cause the extreme blade loads recorded by strain measurements along the root. Figure 4 compares the averaged axial inflow with the instantaneous reversal of the inflow caused by the oscillating ring vortex and Figure 5 shows Jessup's (2004) measurements of the flow's average velocity compared with velocities during an extreme blade loading event.

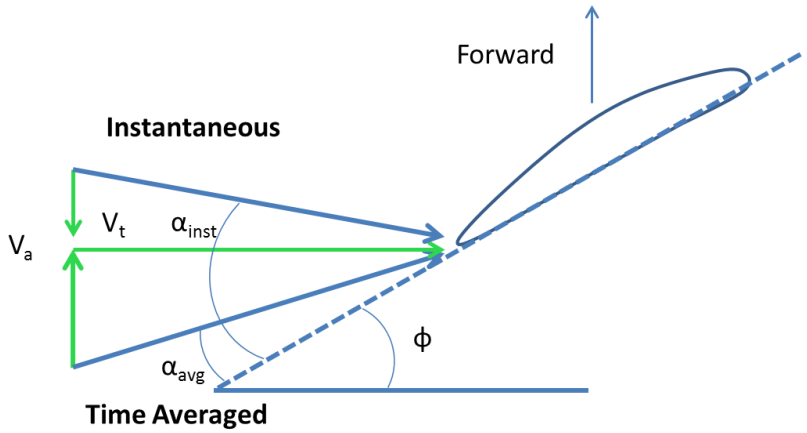

FIGURE 4-CRASHBACK INSTANTEOUS INFLOW AND TIME AVERAGED INFLOW

Images of blade cavitation showed shifting, unsteady patterns along the leading edge of the blade. The irregular cavities were attributed to the stall that occurs when the local tip flow reverses as discussed above. These low pressure cavities add to the extreme, instantaneous blade loading. A blade element approach using solely the extreme axial velocities found that blade thrust was 215% and torque was 188% of the mean crashback state. The root bending moment was 280% greater than the mean due to the excessive tip loading [2].

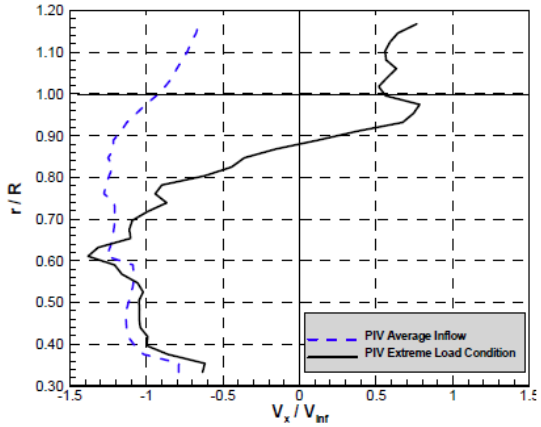

FIGURE 5-CRASHBACK INFLOW VELOCITY COMPARISON (REPRODUCED FROM [2])

NSWC-CD crashback research also analyzed the side forces imparted on the propeller. The primary focus of the effort was to map the asymmetrical behavior of the ring vortex around the propeller disk. Whereas earlier investigations took PIV data from the X-Z plane, the authors now focused on imaging the Y-Z plane to capture the instantaneous unsteady flow over the entire propeller disk. This provided insights into the cross flow through the propeller disk that governs

the side force on the blades and hub. Using shaft dynamometry and tri-axial strain gages on the blade, Jessup et al. (2006) tested at advance coefficients from -0.3 to -1.0. Their findings included strain peaks as high as 3.6 times the average. They confirmed that the region from -0.5 to -0.75 has the greatest amount of unsteadiness, as witnessed in earlier trials. Analysis of the side forces found that they maintain 7-8% magnitude of the average thrust through time. Time-averaged Stereo PIV (SPIV) images of the propeller disk showed a symmetric inward radial flow across the face of the propeller. However, a series of instantaneous images over a three second time period revealed predominantly unsteady, asymmetric flow. Samples of these images are shown below in Figure 6. A longer series of the images shows the flow field rotating around the shaft axis.

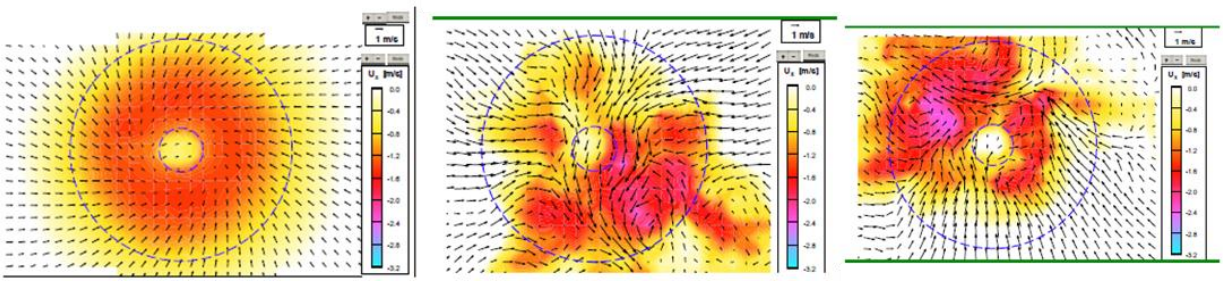

FIGURE 6-TIME AVERAGED AND INSTANTANEOUS PROPELLER DISK FLOW DURING CRASHBACK (REPRODUCED FROM [3])

Adequate computational modeling of the crashback maneuver has been limited because of the large amount of unsteadiness around the propeller disk. Propellers operating in normal ahead or backing conditions are well documented through Reynolds-Averaged Navier-Stokes (RANS) modeling and potential flow models [4]. However, when applied to the highly unsteady flow conditions during crashback, these methods fail to agree with experimental data. Chen & Stern (1999) applied RANS to all four flows around a DTMB 4381 propeller (ahead, backing, crashahead, crashback). While they found good agreement with ahead and backing flows with differences of 5% and 6.5% for thrust and torque predictions respectively, the predictions for the highly turbulent crashahead and crashback flows were 110% different from experimental values. RANS also failed to capture the high amplitude oscillations around the mean thrust and torque measurements by 17%.

Noting the failure of RANS modeling in analyzing propeller crash flows, Mahesh and Vysohlid (2007) applied large eddy simulations (LES) to the problem because of its inherent ability to capture large scale turbulence. Modeling the computational domain and propeller to match that of Jessup's (2004) water tunnel experiments, Mahesh and Vysohlid (2007) simulated crashback conditions over 300 propeller revolutions in order gather more reliable statistics and derive power spectral densities of thrust, torque, side-forces and cross flow. All simulations were run at an advance ratio of J= -0.7 and a Reynolds number of Re = 480,000 defined as

$$J = \frac{U}{Dn} \quad , \quad Re = \frac{DU}{v} \tag{1}$$

Where U is the free-stream velocity, n is the propeller rotational speed in revolutions per time unit, D is the propeller diameter and v is the kinematic viscosity. The calculated thrust and torque revealed large amplitude, low-frequency oscillations, comparing well with Jessup's experiments. Plots of the power spectral densities (PSD) of the simulated and experimental thrust and side force showed good correlation around the frequency of 5 rev^{-1} for thrust and torque. This corresponds to motion of each blade of the five bladed propeller. The lobes and greater spectral density in the experimental values, especially at the higher frequencies, were attributed to blade bending, blade vibration and other resonances of the experimental shafting and machinery [5].

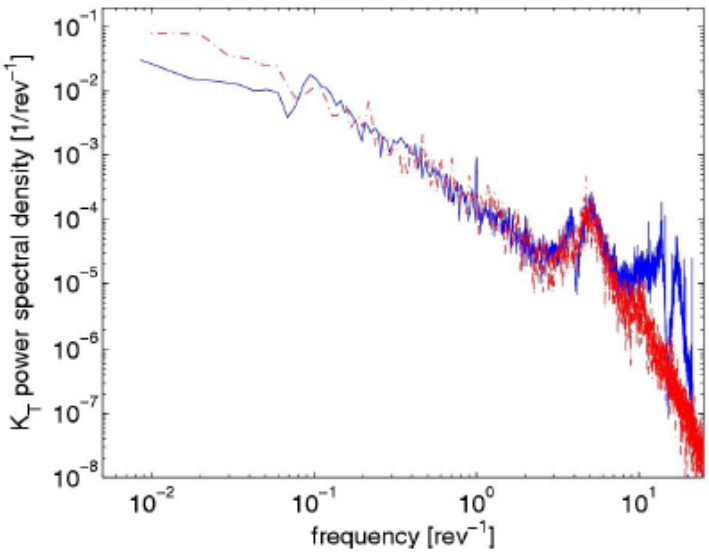

FIGURE 7-THRUST POWER SPECTRAL DENSITY, EXPERIMENTAL IN BLUE, LES SIMULATION IN RED (REPRODUCED FROM [5])

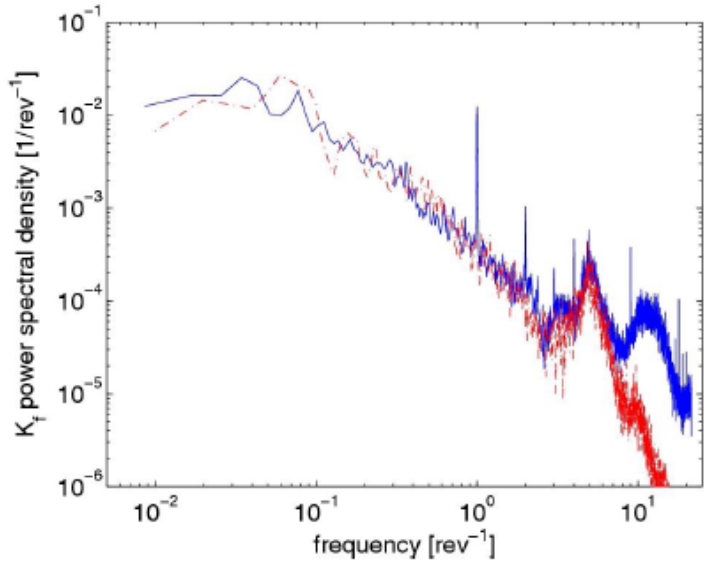

FIGURE 8-SIDE FORCE POWER SPECTRAL DENSITY, EXPERIMENTAL IN BLUE, LES SIMULATION IN RED REPRODUCED FROM [5])

Mahesh's and Vysohlid's (2007) subjective comparison of Jessup's (2006) experimental PIV data and the LES simulations revealed differences in the manifestation of the ring vortex during crashback. While the axial velocities showed good agreement, the ring vortex was closer to the propeller in the simulation than it was in Jessup's experiments. Axial, radial, and tangential velocities all showed high fluctuation in the root mean square (RMS) values with an

exception at the blade tip, where the experimental values showed a much larger RMS fluctuation than was simulated.

The loads during crashback are largely due to the unsteady ring vortex that oscillates upstream and downstream and rotates around the propeller disk plane. A primary difference between the normal ahead operation and the crashback condition is the sign of the pressure differential across the blade face. Whereas in the ahead condition, the high pressure, downstream blade face is pushing the blade in the opposite direction of the free steam, in the crashback condition, the pressure side pushes the blade in the same direction as the free stream [5]. While Mahesh and Vysohlid (2007) validated the use of LES simulations in modeling the crashback condition at steady advance coefficients, further simulation could examine the unsteady load effects during an actual crashback and a dynamic advance coefficient. Prior research on flapping-foil propulsion has revealed that the load effects of unsteady stall and leading edge separation induced by dynamically changing the angle of attack are not trivial [6].

1.1.2 3D Synthetic Aperture Imaging for Fluid Flows

Accurate measurement of fluid flow characteristics around the hull of a ship provides engineers with data to better design the propellers. To ensure the accuracy of the measurements, non-intrusive flow visualization techniques such as LDV and PIV are applied. These methods are used heavily in characterizing propeller and hydrofoil flows in a stationary setup. PIV requires that the fluid be seeded with small particles that trace the flow path. The fluid volume or plane of interest is illuminated, typically with either a laser or a strobe, and high speed cameras capture the motion of the seed particles. Using post processing software, the speed and direction of the particles can be derived. Until the last decade, all PIV was conducted in a stationary manner, where the plane of interest and the body remained fixed in space. To capture the flow field around the hull, the ship model is run past the PIV or LDV setup and an instantaneous, 2D flow field image is captured. The process of repeated, precisely timed runs at various locations is a difficult and time consuming process. Utilizing an optical imagining system that traveled with the model would alleviate these complications as well as provide time averaged and instantaneous flow field data. Two recent attempts have been successful in designing and testing moving PIV systems for measuring velocity fields around the hull of a moving ship model: one at the University of Iowa's tow tank and the other at Taiwan's National

Cheng Kung University's tow tank [7][8]. The difficulty in building such a system lies in the submergence of the laser for illumination of the field of view and actively seeding the fluid ahead of the model without disturbing the flow. Some of the issues noted by the Taiwanese researchers included image distortion due to air entrained by the bow wave of the ship, interference of the hull geometry with the desired laser sheet placement, and shadowing of the images caused by the laser reflecting off the model's bright yellow color. Their setup placed the submerged laser astern of the vessel, facing forward and used a camera above the water surface with the field of view provided by a duct and mirrors [8]. The University of Iowa's setup is similar except that it is designed specifically for their facility and would require a significant amount of re-engineering to incorporate the system into another tow tank. All the lasers and cameras of the Iowa setup are fully submerged in the fluid [7].

While the field of 2D flow imaging is mature, 3D imagining is still seeking advancement. According to Belden (2011), the current state of 3D imaging is limited in resolution and resolvable frame size. A thorough review of three-dimensional flow imaging techniques is discussed by Belden [9]. Additionally, optical occlusions restrict the efficacy of the imaging and, in some instances, the system cannot be extended to multiphase flow problems, such as that of a ship hull, where air has been entrained along the length of the hull due to the bow wave. Belden developed a novel PIV technique incorporating synthetic aperture imaging (SAPIV) to capture 3D fields of view and effectively increase the lens aperture to "see through" partial occlusions. Using an array of several cameras, each captures an image within the field of view, although some parts of the viewport may be occluded. Applying a post processing algorithm that accounts for the depth of the objects due to parallax, the individual images can be refocused on planes within the viewport to reconstruct the 3D space. This method inherently solves the obstruction issue as well as produces a 3D rendering of the event. Figure 9 is a simple schematic explaining the synthetic aperture process taken from Belden's PhD thesis [9]. Belden successfully developed and validated a 3D SAPIV system with moderately dense fluid seeding (0.0266 ppp) but expected that increasing the seeding for better velocity profile resolution would be practical. The capability of the system is scaled by the number and abilities of the imaging cameras used. The largest volume successfully imaged was 100 x 100 x 100 mm^3. Imaging of the highly dynamic crashback event could greatly benefit from this new flow velocimetry technique. During his validation process, Belden successfully imaged a vortex ring which is

fundamentally similar to the vortex ring that develops around the propeller blades during crashback. The potential future application of Belden's SAPIV method to propeller flow visualization with the present ship model drove the need to design a stern window over the propellers and rudders of the model that is discussed later. The acrylic window provides a large enough view port and mounting area for an array of up to nine of the Point Grey Research, Inc. Flea2 cameras.

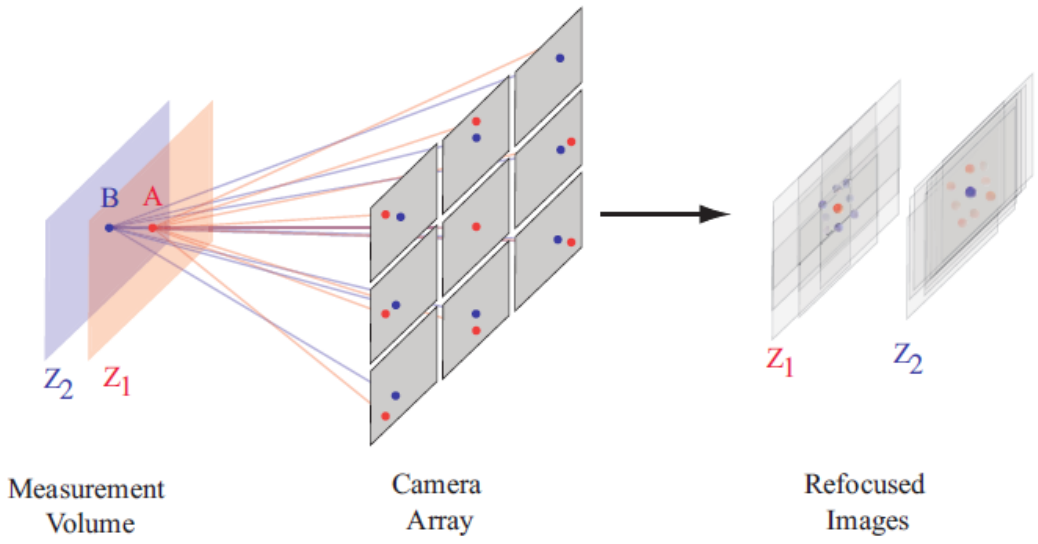

FIGURE 9-SYNTHETIC APERTURE EXAMPLE (REPRODUCED FROM [9])

1.1.3 Free-running Model Testing

Froude-scaled free-running model tests are typically used within the ship design process to evaluate the maneuvering ability and the course keeping ability of the design prior to full scale production. Though costly, this method continues to be an integral part of the design evaluation process. When equipped with precise position and acceleration sensors, the maneuvering and handling characteristics of the model can be measured and scaled to the full scale ship. The International Towing Tank Conference (ITTC) Recommended Procedures and Guidelines outlines the conditions and practices for all scaled model testing. These include water depth effects, model and full scale similitude, scale effects, and the test and analysis procedures. Because the model will be operating in open water, whether it is the Charles River or a local rock quarry, the depth to draft ratio will remain above the minimum value of $^{h}/_{T} = 4$to minimize boundary layer effects [10].

In accordance with the ITTC Recommended Procedures and Guidelines for Ship Models, the bow should be outfitted with turbulence stimulators in the form of studs, wires, or sand grain strips. Turbulence stimulation ensures that both the model and full scale are in the same flow regime and that the model scale flow is consistent and repeatable across the range of evaluated Froude numbers. As well, the stimulators serve as a method of standardization across all model resistance testing. However, the method outlined in [11] for application of turbulence stimulators provides a blanket approach to all ship models and does not recognize the relation between stud size and the model's boundary layer thickness. This method, from Hughes and Allan (1951), is summarized in Figure 10.

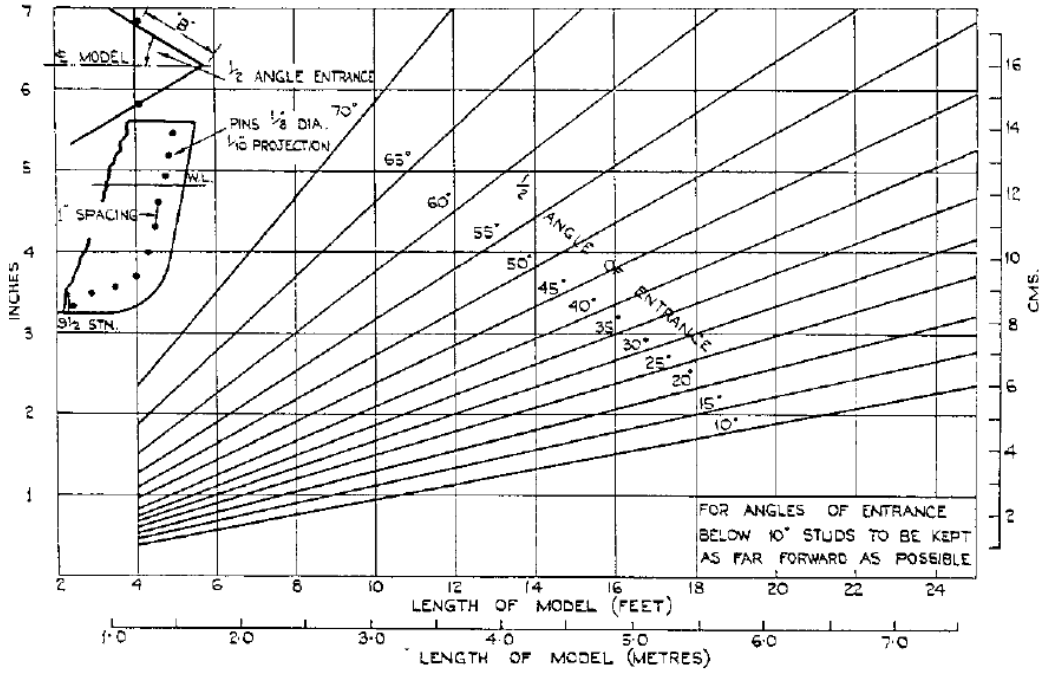

FIGURE 10-HUGHES AND ALLAN TURBULENT STIMULATION METHOD (REPRODUCED FROM [11])

The overarching function of turbulence stimulation is to rapidly trip turbulence at a controlled location along the length of the ship. On full-scale ships operating at a Reynolds number of 10^8or higher, the flow transition will occur at or directly aft of the free stream entry point on the stem. At model scale, however, the natural laminar-turbulent transition is dependent on several factors including the amount of background turbulence, the model surface roughness and upstream boundary layer profile, the presence of flow unsteadiness, surface temperature, and the local streamwise pressure gradient. The dependence of the transition point on these

conditions is mitigated through the use of turbulence stimulators near the water entry point. As well, the stimulator must be of sufficient size to initiate a rapid transition so that the form drag of the model is not significantly altered. This is quantified in a non-dimensional height ratio, y+, of the stimulator to the local boundary layer thickness. y+ values of at least 300 for three-dimensional type (e.g. cylindrical stimulators) is required to achieve a rapid transition [12]. Furthermore, the difference between the desired decrease in laminar skin friction drag and the unwanted increase in form drag due to the application of turbulence stimulation devices to the hull should be considered and calculated using the methods provided in [12]. Turbulence stimulators were not included in the initial design of the model, although it will be operating in a laminar flow condition at a Reynolds number of 9.0×10^6, and should be considered after initial testing and trials.

In addition to the previously mentioned considerations, five conditions must be met in order that the model results accurately represent the full scale handling and maneuvering characteristics as dictated in Principles of Naval Architecture [13].

1. The non-dimensional mass moment of inertia of the model about the z-axis, I_{zz}' should be identical to that of the ship.

2. The model rudder should be deflected to the same maximum angle as the ship rudder at the same non-dimensional deflection rate as that of the ship, i.e.,

$$\dot{\delta}'_{Rm} = \dot{\delta}'_{s} = \frac{\dot{\delta_m} L_m}{V_m} = \frac{\dot{\delta}_s L_s}{V_s} \qquad (2)$$

3. If the ship heel in maneuvers is to be properly simulated, the I_{xx}' of the model as well as its non-dimensional transverse metacentric height must be identical to that of the ship. (In practice, these are difficult conditions to fulfill.)

4. The model propeller operating slip ratio should be identical to the ship propeller slip ratio. This is particularly important if the rudder is located in the propeller race.

5. If the speed loss in maneuvers is to be properly simulated, the response of the motor that drives the model propeller to an augment in model resistance should duplicate the response of the power plant of the full-scale ship to a corresponding augment in ship resistance.

Adherence to and deviation from these scaling laws is discussed in Chapter 2. Recommended trial and testing procedures are outlined in [10].

1.2 Project Goals

The primary goal of this project was to design and build a 1/30th scale, free-running model of the David Taylor Model Basin hull for hydrodynamic visualization and crashback maneuver testing. Because of the desired scale, the model will be utilized in open water, e.g. the Charles River, Boston Harbor, or a local rock quarry. The model will serve as a flexible test platform for future research within the MIT Ocean Engineering department.

2 MODEL DESIGN

2.1 DTMB 5415

2.1.1 Hull Background

The David Taylor Model Basin 5414 was developed as the preliminary hull form for the U.S. Navy Aegis guided missile destroyer program in the early 1980's. The hull is characterized by a bulbous SONAR dome on the bow and a transom stern. Propulsion is provided through two shaft lines. The design speed is defined as 20 knots (33.8 m/s) at full scale. Though no full scale ship has ever been built to the 5415's exact lines, the hull served as the precursor to the DDG 51 Arleigh Burke class of naval vessels that is currently comprised of 61 ships and has set the standard for large naval surface combatants. The lines are shown in Figure 11.

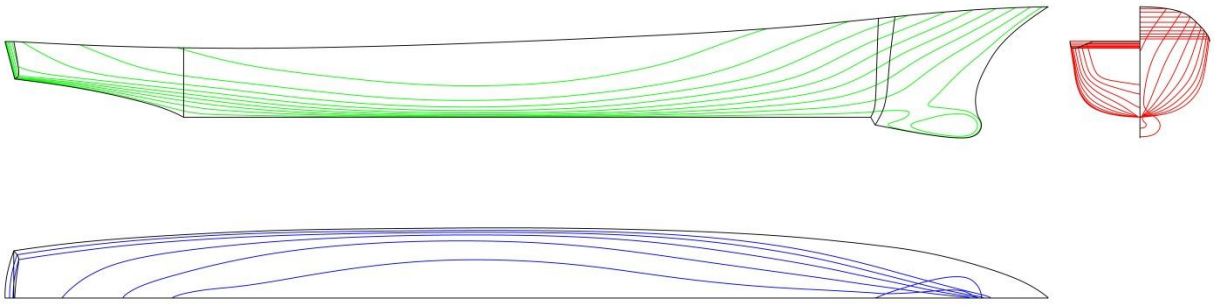

FIGURE 11-DAVID TAYLOR MODEL BASIN 5415 LINES

The hull form has become ubiquitous in naval architecture circles and has been the subject of extensive hydrodynamic testing and validation over the past several decades. Ongoing research

has relied upon the well documented tow tank resistance and planar motion mechanism testing to validate Computational Fluid Dynamics (CFD) codes. The Workshop on Verification and Validation of Ship Maneuvering Simulation Methods (SIMMAN 2008) is an ongoing effort to validate computational codes with experimentally measured data on several hull forms, including the DTMB 5415[14][15][16][17]. The complex underwater hull geometry lends itself to these validation efforts. The general particulars of the full scale hull and model scale are provided in Table 1.

2.1.1 Scaled Hull Specifics

Aside from the following adjustments, the model hull is a $1/30^{th}$ scaled model of the DTMB 5415. Early in the design phase, it was decided to omit the bilge keels from the scaled hull form, the primary reason being that they would be highly susceptible to damage during launching operations. Another consideration that had to be made was that the model would be operating in an open water environment where environmental conditions could not be controlled. To mitigate the risk of potentially flooding and swamping the boat, the sheer line was raised to increase the freeboard. Creating a flat surface also allowed for a plexiglass lid that would seal the internal compartments from flooding. The main particulars of the model and full scale DTMB 5415 are shown in Table 1.

TABLE 1-DTMB 5415 FULL SCALE PARTICULARS [18]

Scale (λ)	1.00	30.0	
Main Particulars			
LWL	466.50	15.6	[ft]
BWL	62.50	2.1	[ft]
T	20.20	0.67	[ft]
Displacement	29,750.90	10.83	[ft^3]
Wetted Surface	31,996.80	36.64	[ft^2]
LCB (%LWL aft of FP)	-0.68	-0.68	
C_B	0.507	0.507	
C_M	0.821	0.821	
Rudders			
Type	Spade	Spade	
Wetted Surface	165.80	0.411	[ft^2]
Turn rate	9.0	49.3	[deg/s]
Propellers			
Type	Fixed Pitch	Fixed Pitch	
Geometry	4876/4877	Modified 4381	
No. of blades	5	5	
Diameter	17	6.8	[ft]
Appendages			
Bilge keels	Yes	No	
Stabilizing fins	No	No	
Test Condition			
Draft	20.20	0.67	[ft]
LCG	-2.14	-	[ft aft MS]
GM	6.40	-	[ft]
ixx/B	0.37	-	
izz/LBP	0.25	-	
Design Speed	33.8	6.23	[ft/s]
Froude Number[ł]	0.28	0.28	

ł Fn at design speed and L = LWL, g = 32.2 ft/s^2

2.2 Model Design and Construction Process

2.2.1 General Model Design

The initial design of the model was conducted in Solidworks and included three windows along the length of the hull for flow visualization. The three windows were positioned so as to be directly aft of known locations of vortex generation. Preliminary quotes received from potential model builders showed that inclusion of all three windows would be cost prohibitive and it was decided that only the stern window would be included in the final design. Figure 12 shows the initial design with the three windows along the length of the hull and Figure 13 shows the location of the stern window in relation to the propellers and rudders. The shaft struts were positioned forward of the intended design location to not interfere with the window. However, this was changed in the final design when a method was devised to support the struts in their originally intended location without interfering with the window. The initial stern window viewport over the propellers and rudders is shown in Figure 14 and the preliminary layout of the internal electronics and batteries including a notional SAPIV camera array is shown in Figure 15.

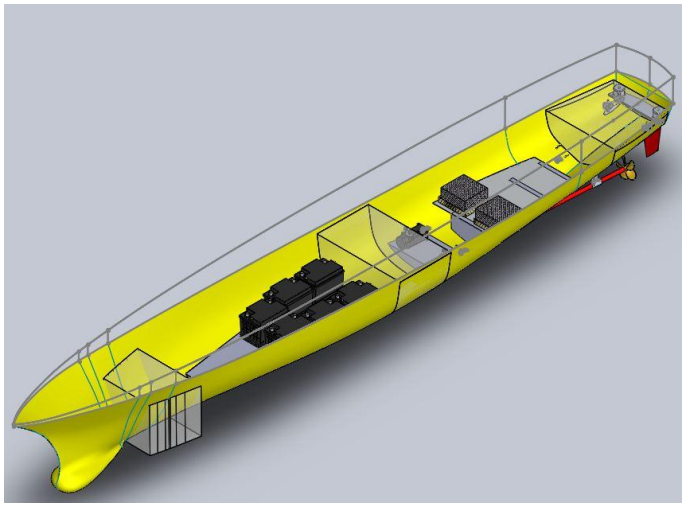

FIGURE 12-INITIAL DESIGN WITH THREE FLOW VISUALIZATION WINDOWS

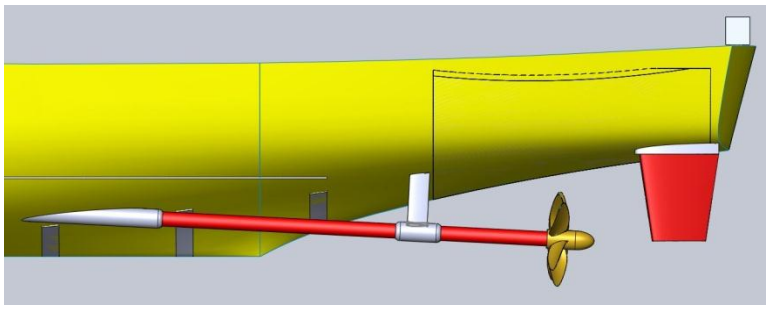

FIGURE 13-STERN WINDOW LOCATION

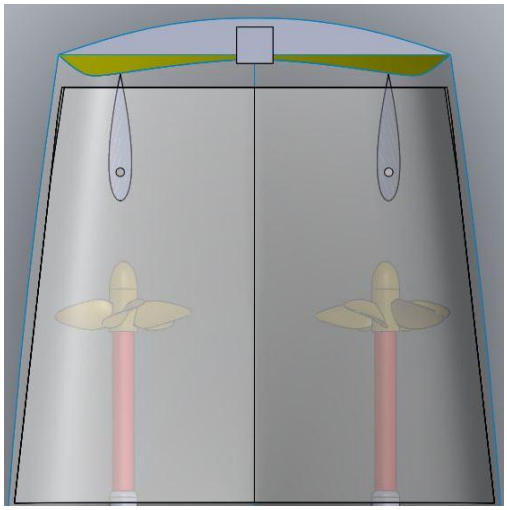

FIGURE 14-INITIAL STERN WINDOW VIEWPORT

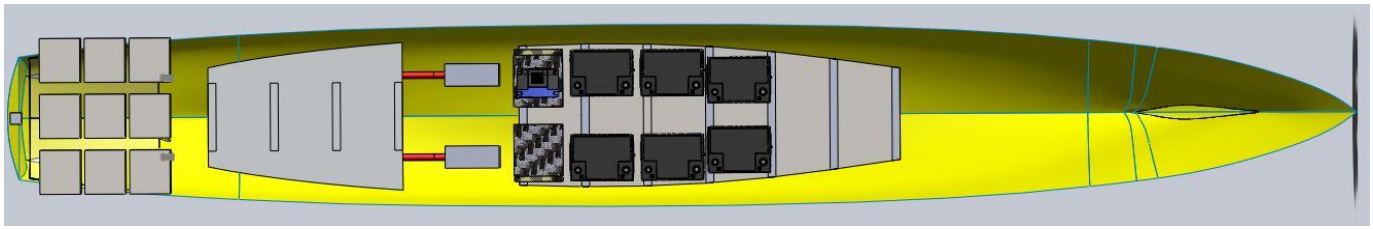

FIGURE 15-NOTIONAL INTERNAL EQUIPMENT LAYOUT

As built, the model has four separate compartments separated by three transverse bulkheads. The forward compartment does not hold any internal equipment. The second compartment houses the batteries and power conversion equipment while the third houses the motor controller, the servo motors, and the servo motor drives. The aft most compartment houses the stepper motors and rudder post assemblies. A schematic of the generic internal system configuration is shown in Appendix F.

FIGURE 16-ISOMETRIC VIEW OF MODEL AS BUILT

2.2.2 Propulsion

Design of the propeller for the model presented several issues. To achieve the best possible efficiency, the propeller is designed to a single vessel speed of advance. At that speed of advance, each vessel's wake, and thus propeller velocity inflow, profile is different. The pitch of the blade sections can then be shifted to the ideal angle of attack to provide the most thrust. For the DTMB 5415 model, the wake profile was publically available (Chesnakas and Ratcliffe 2005). In their research, the wake profile of a 1:24.824 scaled DTMB 5415 model at 20 knots full scale was measured using LDV methods. Testing was conducted both under un-propelled and propelled conditions at several axial locations along the shaft in the vicinity of the propeller. For the propelled condition, the DTMB propellers 4876 and 4877 were used. These are a set of high skew, opposing direction (left and right handed) propellers designed for the DTMB 5415. Figure 17 is an image of the stern of Chesnakas' and Ratcliffe's (2005) model with the 4876 and 4877 propellers. Figure 18 shows the contours of axial wake velocity at x/L of 0.9603 and Figure 19 shows the propelled axial velocity contours at x/L of 0.9603.

FIGURE 17-DTMB 4876 AND 4877 PROPELLERS ON DTMB 5415 MODEL (REPRODUCED FROM [19])

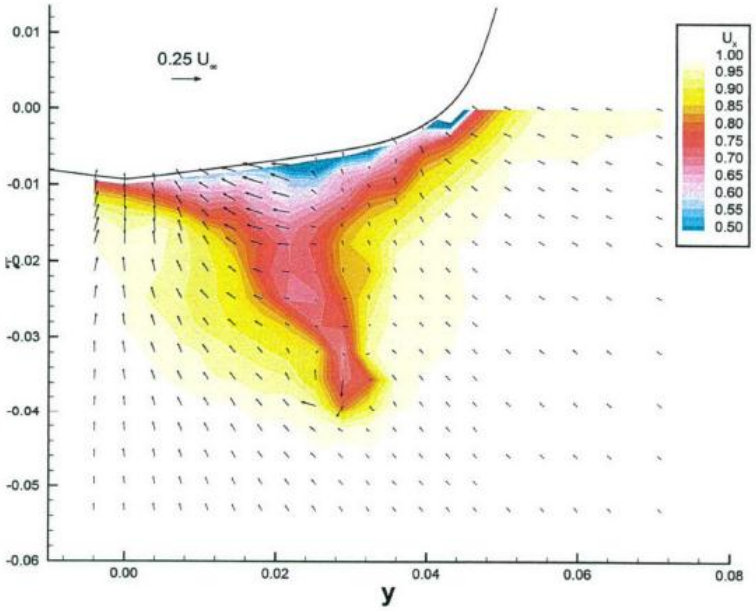

FIGURE 18-CONTOURS OF AXIAL VELOCITY, X/L = 0.9603, NOMINAL WAKE (REPRODUCED FROM [19])

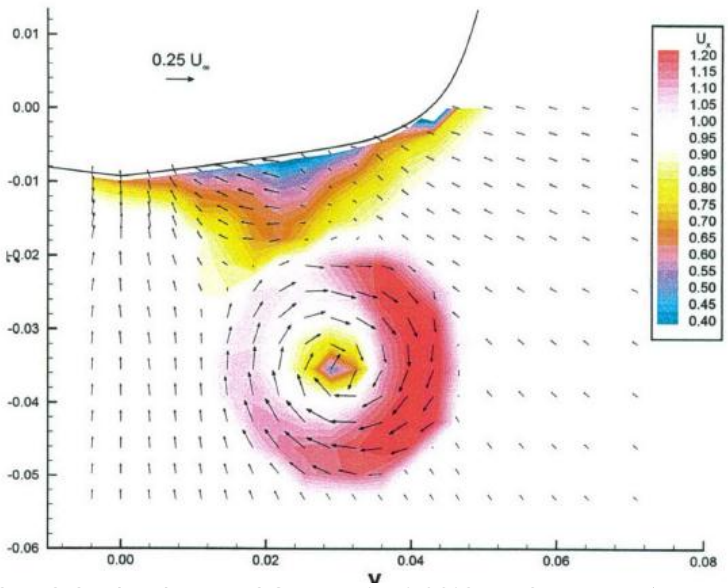

FIGURE 19-CONTOURS OF AXIAL VELOCITY, X/L=0.9603, PROPELLED (REPRODUCED FROM [19])

What can be seen, especially in the nominal wake profile, is the interaction of the strut and shaft wakes. Applying this measured profile to the DTMB 5415 of this project would neglect the importance of this interaction since the struts for the model had to be adjusted from the initial design to accommodate the aft window.

The option of adopting the DTMB 4876 and 4877 propellers that were utilized in Chesnakas and Radcliffe (2005), as well as other DTMB 5415 studies, was considered for the 1:30 model. However, while the geometries were available, no four quadrant flow data was available. Because one of the primary areas of initial research for the model is the crashback maneuver, not having the full four quadrant data on the propellers would require a separate series of water tunnel tests to measure and document their open water characteristics. Therefore, propeller 4381, a well-tested and heavily documented propeller, was decided upon as the initial propeller for the model. The DTMB 4381 is a spade type propeller with zero rake and zero skew. To maintain the geometric similarity between the model and full scale, each of the propellers was linearly scaled using the same factor as the hull form, resulting in a diameter of 6.8 inches assuming a full scale DDG 51 propeller diameter of 17 feet. As with all scale model testing, it is desirable to minimize the ratio of full scale to model scale, although in practice this is hardly achievable. In order to gather accurate thrust and torque measurements of scaled propellers, the propellers must be sufficiently large to mitigate scale effects associated with low Reynolds numbers. Laminar flow around the propeller blades has been witnessed even during

moderately large model scale self-propulsion tests. Principles of Naval Architecture recommends that because of the aforementioned scale effects, the model scale propeller diameter should be no less than 8 inches and preferably closer to 16 inches. In terms of Reynolds numbers based on blade chord length at the 0.7 radii, the lowest acceptable figure is 4 x 10^6. However, if turbulence stimulation is present on the leading edge of the propeller blade, then the propeller operating Reynolds number should be no less than 3 x 10^5 [20]. The velocity of the blade is calculated as shown in Equation 3.

$$V = [(0.7\pi nD)^2 + (V_a)^2]^{1/2} \tag{3}$$

With a geometrically scaled DTMB 4381 propeller diameter of 6.8 inches, the Reynolds number at the design Froude number of 0.28 is 5.38 x 10^5, below the non-turbulence stimulation limit but well within the limit set forth by the 1975 ITTC mentioned above for blades with turbulence stimulation. As will be seen below, the method of manufacturing the initial prototype propellers resulted in sufficient roughness along the leading edge to justify application of the lower Reynolds number limit. Another consideration is the previously cited requirement that the propeller slip ratios of the full scale ship and the model be identical. Assuming that the full scale ship would use a propeller geometry similar to the DTMB 4876/4877 with a pitch to diameter ratio (P/D) of 1.549 and a nominal design shaft revolution speed of 100 RPM, the slip ratio, s_r, of a full scale DTMB 5415 would be approximately 0.4205. Slip ratio is calculated as

$$s_r = 1 - \frac{V_a}{Pn} \tag{4}$$

where *P* is the pitch of the propeller at the 0.7 radii and *n* is the propeller rotational speed in revolutions per second. The P/D for the 4381 propellers is 1.21 and the nominal shaft speed at the design speed (Fr = 0.28) is 696 RPM. This results in a propeller slip ratio of 0.3734. Although the ratios are not identical, the full scale data relies on several assumptions. The model shaft RPM is based on theory and not the actual performance of the system and future iterations of the propellers will have a higher pitch to diameter ratio.

For the initial propeller manufacturing iteration, the cost was significantly reduced by fused deposition modeling (a form of 3D printing) them in ABS-M30 plastic. Previous experience in 3D printing of plastic propeller blades had shown a limiting blade thickness of approximately 0.08 inches for ensuring the trailing edges were printed solid. The blade thickness profile of the DTMB 4381 was adjusted to meet this requirement and the resulting blade thickness versus radius profile is shown in Figure 20. Changing the thickness profile changes the operating characteristics of the propeller. The effects were thought to be negligible for the first iteration of the design. If required for future experimentation, a more accurate representation of the 4381 should be constructed. Figure 21shows the C_T and $10C_q$ versus β, the hydrodynamic pitch angle. This method of presentation captures the entire range of operation of the propeller and averts the issues caused by the advance ratio, J, going to infinity when the propeller speed approaches zero.

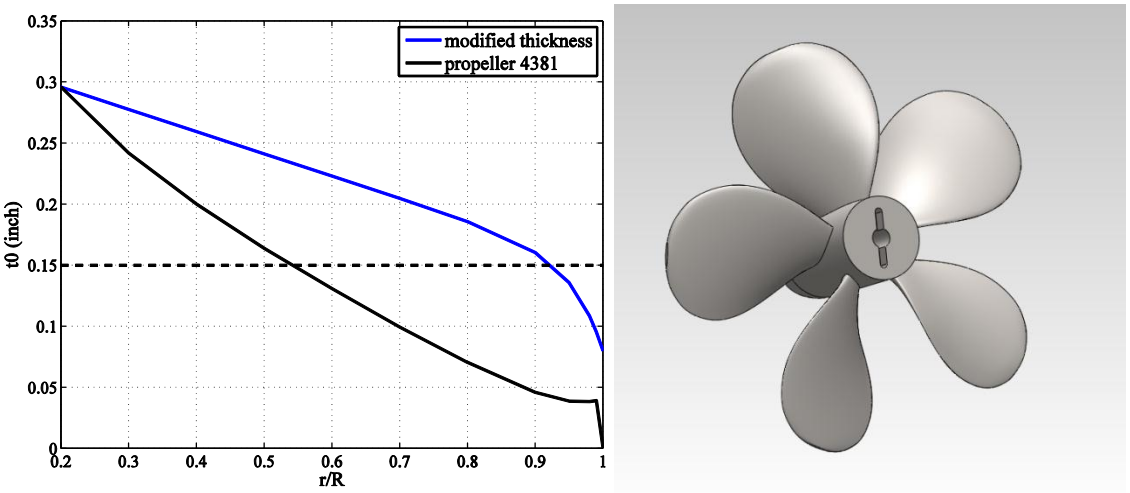

FIGURE 20-MODIFIED BLADE THICKNESS PROFILE AND SOLIDWORKS RENDERING OF PROPELLER 4381

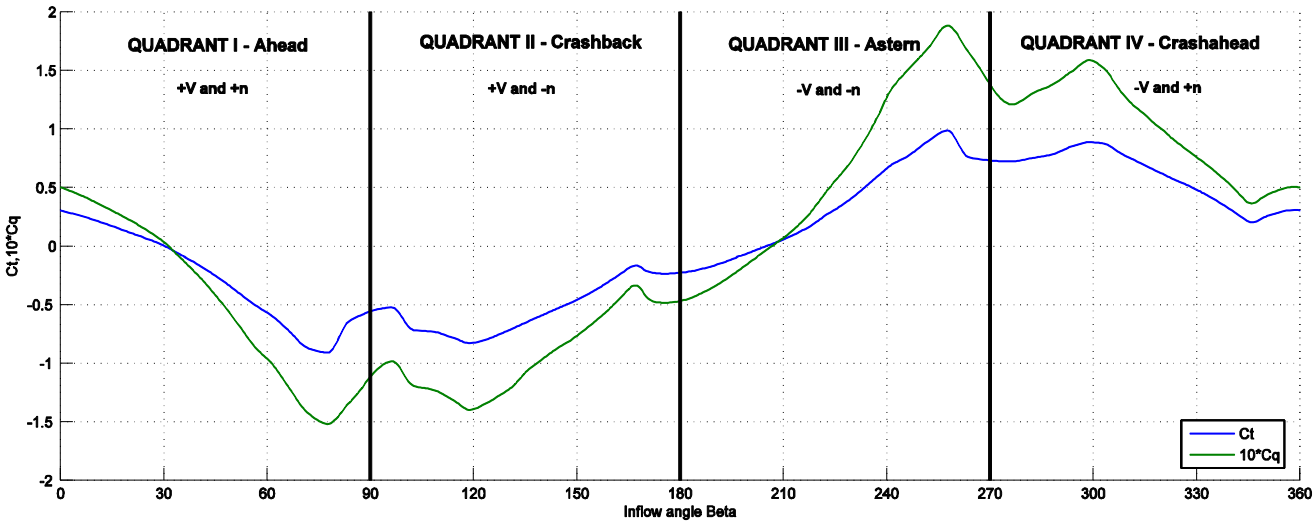

FIGURE 21-FULL FOUR QUADRANT DATA FOR PROPELLER 4381

The water permeability and stiffness of the ABS plastic was addressed by copper-nickel plating the propellers. This technique for producing low cost, accurate and durable model propellers has been utilized by Naval Surface Warfare Center, Carderock Division (NSWC-CR). The same rapid prototyping company used by NSWC-CR, RePliForm Inc., was contracted to plate the two DTMB 4381 model propellers for the project using their proprietary RePliKote technique. The total plating thickness, including both the copper and nickel layers, amounted to 0.004 inches or approximately 102 microns. Table 2shows the relative blade stiffness increase due to plating the propeller blade as well as a solid aluminum blade.

TABLE 2-RELATIVE BLADE STIFFNESS AT 0.72 BLADE RADIUS

Blade Material	Young's Modulus (E)	2nd Moment of Area (I)	EI	Relative Stiffness
ABS FDM	1.45 x 10^5 [psi][1]	7.77E-04 [in^4]	1.13E+02[lb-in^2]	1
Cu+Ni Plated ABS	3.0 x 10^7 [psi]	8.74E-04 [in^4]	3.01E+03[lb-in^2]	27
Solid Aluminum	1.0 x 10^7 [psi]	7.77E-04 [in^4]	7.77E+03[lb-in^2]	69

[1][32]

An off-design analysis of the propeller was conducted to provide a starting point for tuning the propulsion motors during initial open water trials. The thrust coefficient required for the model at each of the off-design speeds was calculated and plotted against the propeller curves. The intersection of the propeller thrust coefficient, K_{T_Prop}, with the model thrust coefficient, K_{T_Model} provides the operating advance coefficient, $J_{off-design}$ from which the required shaft RPM can be calculated. The model thrust coefficient was calculated by

$$K_{T\_Model} = \frac{1}{\rho D^2} \cdot \frac{c_1}{k_p(1-t)(1-w)^2} \tag{5}$$

$$c_1 = \frac{R_{Tm}}{V_m{}^2} \tag{6}$$

where R_{Tm} is the effective resistance of the model. The thrust and wake factors, *t* and *w* respectively, were assumed constant although in reality these change slightly with ship speed. The intersecting K_{T_Model} and K_{T_Prop} curves are shown in Figure 22 and the required propeller RPM versus full scale ship ahead speed is shown in Figure 23.Table 3 shows required propeller speeds at selected model and equivalent ship speeds.

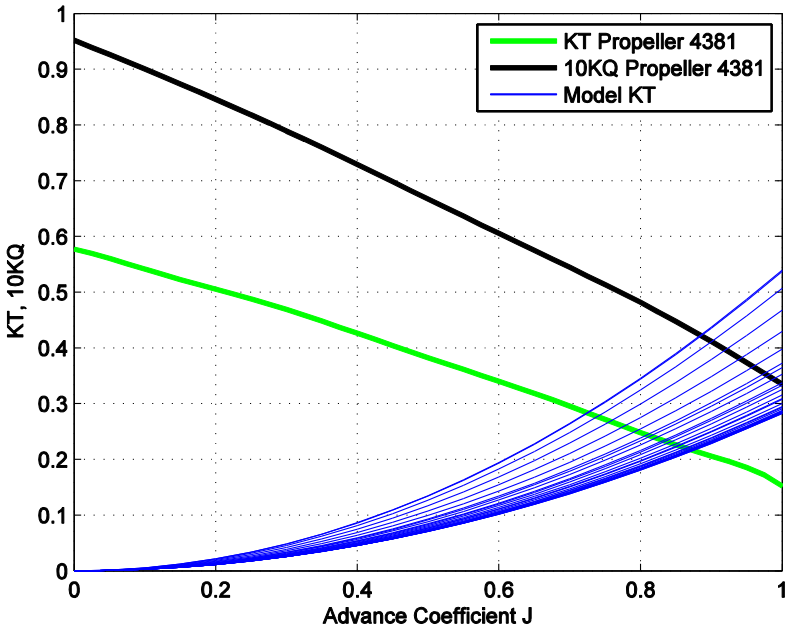

FIGURE 22-OFF-DESIGN PROPELLER SPEED ANALYSIS. NOTE SAME DATA AS FIG 17, QUADRANT 1 (0<B<90)

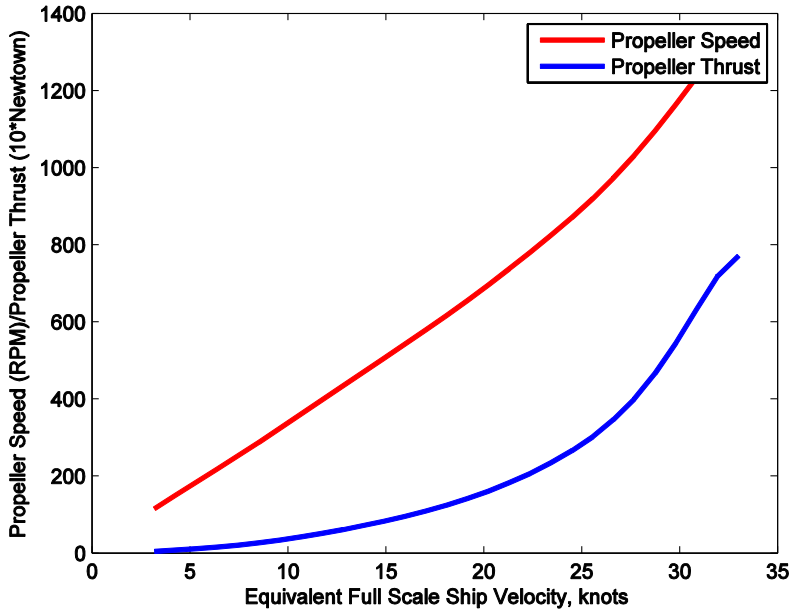

FIGURE 23-REQUIRED PROPELLER RPM AND DELIVERED THRUST

TABLE 3-REQUIRED PROPELLER RPM AT SELECTED SPEEDS

Fr	V_{ship}	V_{model}	N_{model}
-	[kts]	[ft/s]	[RPM]
0.073	5.32	1.64	185
0.132	9.58	2.95	324
0.205	14.91	4.59	506
0.279	20.23	6.23	696
0.338	24.49	7.55	870
0.411	29.81	9.19	1,164

2.2.3 Maneuvering

Because of the Froude scaling, the full scale Reynolds number of the ship cannot be simulated. The significance of this failure in similitude is witnessed in the maximum lift and stall angles of foils. Froude similitude requires that the model speed be less than the full scale speed, making the Reynolds number for the model rudder much less than the full scale and typically within the laminar flow region. For this project, the Reynolds number of the full scale (Re_s) DTMB 5415 is 2.2 x 10^9 whereas the model Reynolds number (Re_m) is 9.0 x 10^6 when

operating at a full scale design speed of 20 knots (Fr = 0.28). The effects that have been identified through wind tunnel testing on standard NACA foils are listed in the Principles of Naval Architecture, Volume III as

1. Maximum lift coefficient increases with Reynolds number because of the delay of stall angle.
2. Lift curve slope varies little with Reynolds number (also with section shape).
3. Drag coefficient decreases with increase of Reynolds number [13].

Also complicating the matter is the surface roughness effects on maximum lift coefficient. If operating at very low Reynolds numbers, the flow around the rudder could be laminar. Laminar flow, being more susceptible to separation, can be the cause of decreasing stall angles in model rudder tests. For Froude scaled models, purely geometric scaling of the rudder will result in a conservative assessment of the rudder's maximum lift coefficient, and thus the ship's turning ability.

Another scale effect that presents an issue for models equipped with multiple rudders is the difference in the full scale and model scale ratio of propeller race velocity to the free-stream. This ratio is much larger for model scale than full scale and is another Reynolds effect. The ratios differ because the much smaller Re_m results in a higher drag coefficient for the model and, in turn, requires the model propeller to operate at a higher slip ratio than the full scale propeller. As with the other Reynolds number effects, this lends to a conservative assessment of the ships maneuvering abilities [13].

The exact specifications of the DTMB 5415 rudder were not available during the design stage of the project model. The only available information was the extents of the projected shape and the placement along the hull, as shown in Figure 24. The design drawings showed the two rudders canted several degrees outboard.

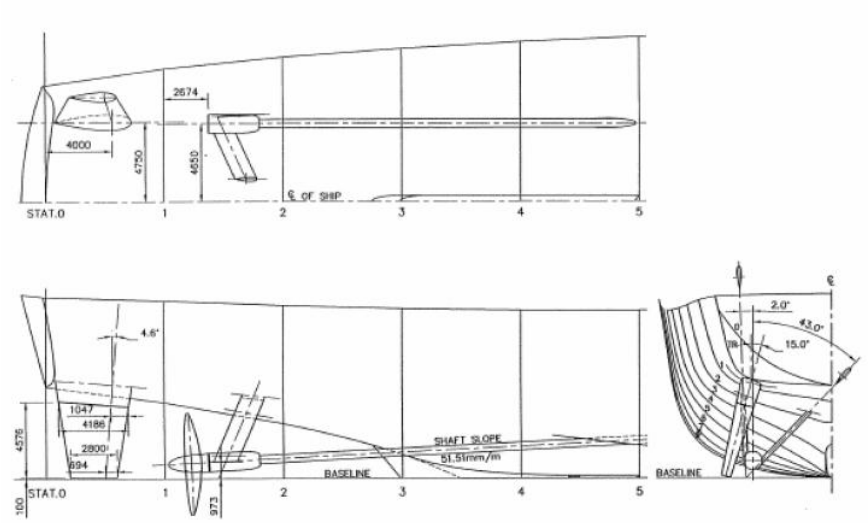

FIGURE 24-DTMB 5415 STERN ARRANGEMENT AS DESIGNED (REPRODUCED FROM [18])

To simplify the mechanics of the system, the cant was removed and the rudders were placed vertically in the same longitudinal position as the drawings. The rudder sections were constructed using a NACA 0018 foil because it has relatively constant center of pressure and the thickness ratio allows for adequate foil strength while maintaining reasonable drag characteristics [13]. The aspect ratio, sweep angle and general extents of the foil projected in the centerline plane were maintained from the drawings. The rudders' general characteristics are shown in Table 4.

TABLE 4-RUDDER DESIGN CHARACTERISTICS

Section Geometry	NACA 0018	
Sweep Angle	4.6	[deg]
Span	0.518	[ft]
Chord (r/R=0.5)	0.381	[ft]
Surface Area	0.411	[ft^2]
Rudder position aft of midships	7.64	[ft]
Effective Aspect Ratio	2.74	
Hoerner Lift Slope $\left(\frac{\partial Cl}{\partial \alpha}\right)_{\alpha=0}$	3.17	

Another deviation from the original design was the arrangement of the propeller struts and fairwater. The initial design used Figure 24 as the starting point for the strut placement and angles. However, securing the struts to the aft window proved difficult during construction and required additional structure that obscured the field of view of the window. To mitigate the structural concerns the outboard struts were rotated to be parallel with the center plane of the hull, allowing them to terminate in the hull structure instead of the window. The field of view over the window was preserved by terminating the inboard struts at a longitudinally placed member that was secured to the hull structure forward of the window. This new configuration is shown in Figure 25.

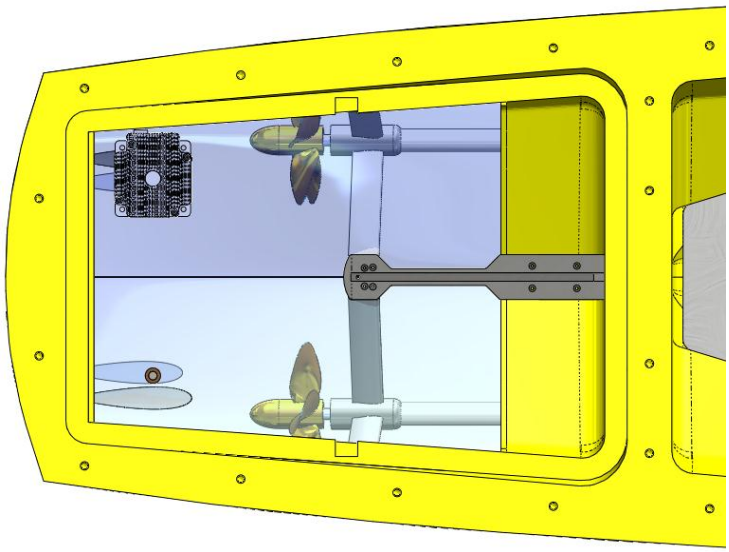

FIGURE 25-FINAL STRUT CONFIGURATION

The estimated steady turning radius of the model was determined using the method outlined in the Principles of Naval Architecture with the orientation shown in Figure 26.

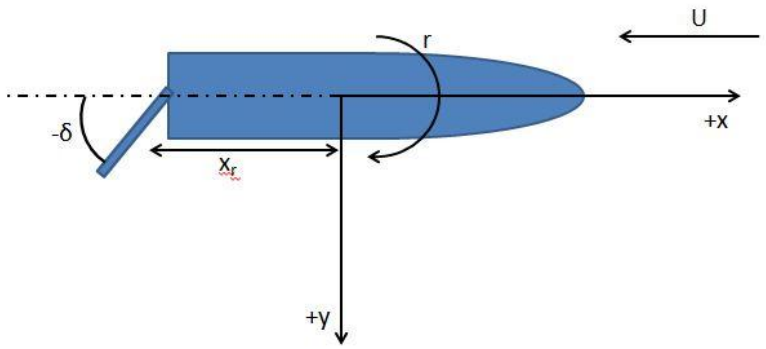

FIGURE 26-SHIP AND RUDDER ORIENTATION DURING A STEADY TURN

Once the vessel in a turn has reached a state of equilibrium, the ship maintains a steady turning radius with *v* and *r* having constant, nonzero values and $\dot{v}$ and $\dot{r}$ being zero. This is known as the third phase of the turning maneuver. The linearized equations of motion taken from Principles of Naval Architecture for a steady turn are:

$$-Y_v v - (Y_r - \Delta' u_1) r = Y_\delta \delta_R \tag{7}$$

$$-N_v v - N_r r = N_\delta \delta_R \tag{8}$$

The linear hydrodynamic derivatives of the DTMB 5415 were taken from the averages of the three research institutions participating in the SIMMAN 2008 workshop. The rudder derivatives were calculated using Hoerner's method for foils at angles of attack below the stall angle. Because the foil aspect ratio is a strong determinant of performance, the slope of the lift coefficient with respect to angle of attack can be found as shown in Equation 9. This is valid for foils with an aspect ratio greater than 1.

$$\left(\frac{\partial Cl}{\partial \alpha}\right)_{\alpha=0} = \frac{1}{\frac{1}{2\pi\bar{\alpha}} + \frac{1}{\pi(AR_{eff})} + \frac{1}{2\pi(AR_{eff})^2}} \tag{9}$$

The effective aspect ratio (AR_{eff}) is twice the standard aspect ratio because of the reflection introduced by the hull of the ship.

$$AR_{eff} = 2 \cdot AR = 2 \cdot \frac{span}{chord} \approx 2.72 > 1 \tag{10}$$

The standard value for $\bar{\alpha}$ is 0.9. Once Equations 7 and 8 are solved for *v* and *r*, and knowing the control derivatives and stability derivatives, and recognizing that $r' \equiv \psi = \dot{r}L/V$ and the steady turning radius $R = V/r$, then $r' = L/R$, the turning radius, *R*, can be found as

$$R = \frac{-L}{\delta_R}\left[\frac{Y_v(N_r) - N_v(Y_r - \Delta)}{Y_v N_\delta - N_v Y_\delta}\right] \tag{11}$$

In addition to the rudder term, Y_δ, the lift force of the rudder generates separate hydrodynamic terms that alter the bare hull terms found in the SIMMAN 2008 data. The total lift generated by the rudders is:

$$\begin{aligned} Y_R = -L &= -\frac{1}{2}\rho A_R U^2 \frac{\partial Cl}{\partial \alpha}\left(\delta_R + \frac{x_r r}{U} + \frac{v}{U}\right) \\ &= Y_\delta \delta_R + Y_{Rr} r + Y_{Rv} v \end{aligned} \tag{12}$$

where

$$Y_\delta = -\frac{1}{2}\rho A_R U^2 \frac{\partial Cl}{\partial \alpha} \tag{13}$$

$$Y_{Rr} = \frac{Y_\delta x_r}{U} \tag{14}$$

$$Y_{Rv} = \frac{Y_\delta}{U} \tag{15}$$

The resulting hydrodynamic moment on the rudder from the rudder lift force is:

$$N = Y x_r = N_\delta \delta + N_{Rr} r + N_{Rv} v \tag{16}$$

where

$$N_\delta = Y_\delta x_r \tag{17}$$
$$N_{Rr} = Y_{Rr} x_r \tag{18}$$
$$N_{Rv} = Y_{Rv} x_r \tag{19}$$

Accounting for this correction in the bare coefficients, the steady turning radius versus rudder angle at the full scale design speed of 20 knots is plotted in Figure 27. Note that a negative

rudder angle, as defined in Figure 26, results in a turn to starboard as would be expected of a stable hull form.

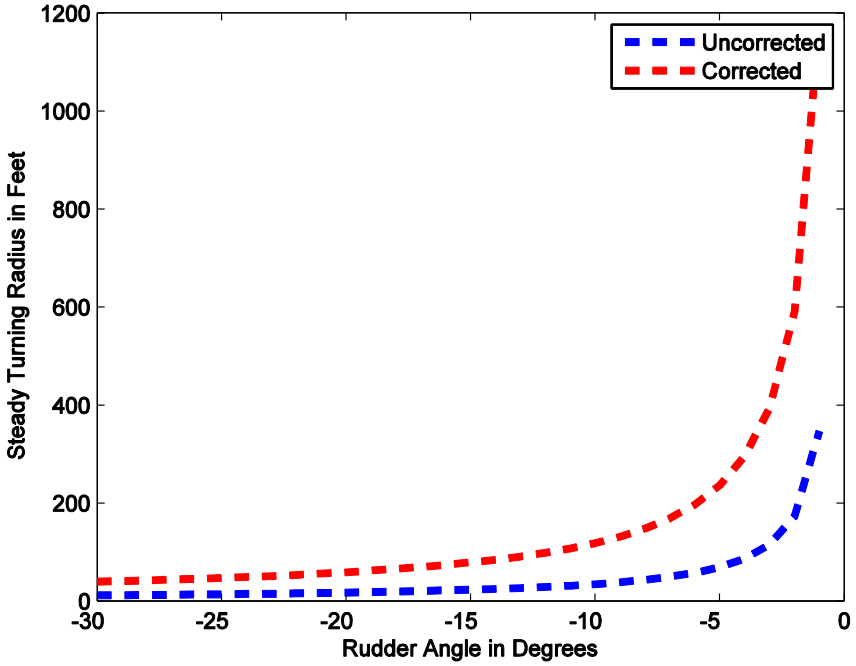

FIGURE 27-MODEL STABLE TURNING RADIUS VERSUS RUDDER ANGLE AT FULL SCALE SPEED OF 20 KNOTS

Using the nondimensional rudder deflection rate scaling requirement discussed above in the modeling, the tandem rudders of the model have to slew at a rate of 0.861 radians per second, or 49.3 degrees per second. Because of the 1:2 stepper motor to rudder sprocket gear ratio, the speed of the stepper motors on the onboard controller were set to twice the deflection rate, or 98.6 degrees per second. Prior to selecting the stepper motors, the approximate holding torque requirements were calculated using the Harrington method outline in Principles of Naval Architecture, Volume III.

2.2.4 Powering

Typically, when designing the power train of a ship, the designer begins with the towed, or effective, resistance of the hull scaled from model tests in a tow tank. Because of the large scale of the model being built and the lack of facilities available to conduct resistance testing,

data was taken from previous studies on the DTMB 5415 hull form. The studies were from Naval Surface Warfare Center Carderock Division and the University of Iowa's Hydroscience and Engineering College. Each data set was scaled to full scale using Froude's technique and plotted against each other, shown in Figure 28. Equation 20 is Froude's Hypothesis where C_D is the total drag coefficient, C_f is the frictional drag coefficient dependent on the Reynolds number, and C_R is the residual drag dependent on the Froude number.

$$C_D(R_e, F_r) \approx C_f(R_e) + C_R(F_r) \tag{20}$$

The INSEAN line is from the University of Iowa, the NSWC-CD line is from a 1984 Navy tow tank analysis and the Tsai line depicts the towed resistance of the full scale DDG 51 hull after changes were made to the initial stern design.

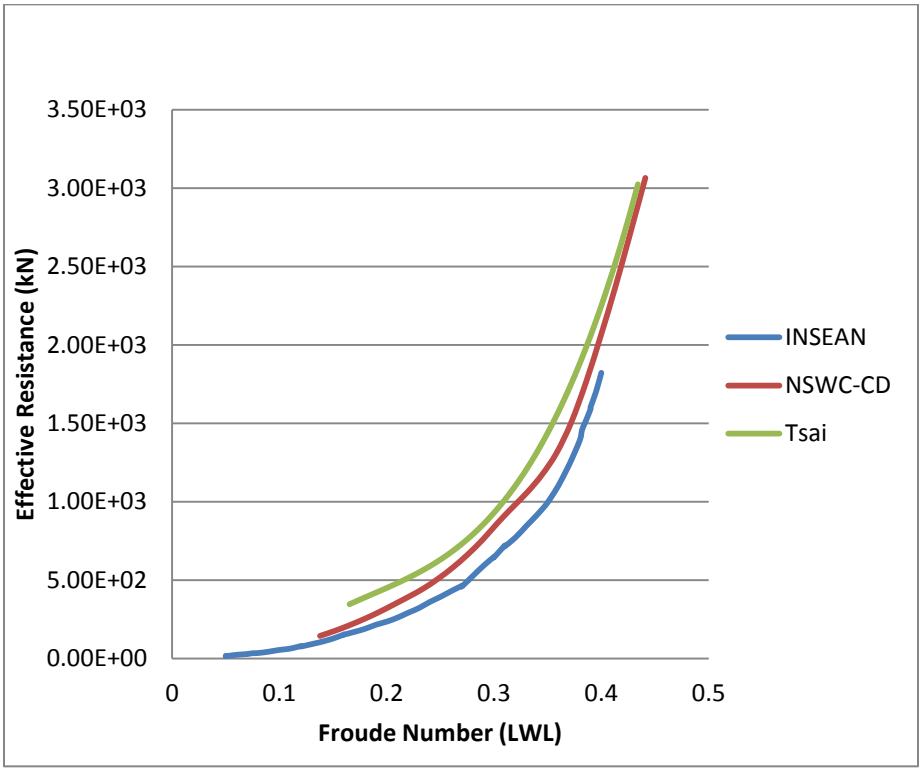

FIGURE 28-FULL SCALE DTMB 5415 EFFECTIVE RESISTANCE COMPARISON

The DTMB 5415 test models were at a scale of 1:24.824 and both utilized turbulence inducing studs on the bow. NSWC-CD used a correlation allowance of 0.0004and the 1957

ITTC Ship-Model Correlation Line. Data was taken from "Experiment 33," in which the hull was fully appended, rudders were placed at 0 degrees from the centerline, and no propellers were installed. The displacement and draft conditions were the same of the design model. The primary goal of the NSWC-CD research was to determine the optimum propeller rotation direction (e.g. inboard or outboard) the effects on hull efficiency of the proposed stern wedge for the DDG 51 class and overall appendage resistance. The study concluded that changing the propeller rotation from inboard to outboard reduced the necessary power delivered to reach 30 knots by 4.0 percent and the shaft revolution rate by 0.6 percent. As well, the stern wedge reduced the required power at 30 knots by 6.7 percent and shaft revolution rate by 1.9 percent. The study also concluded that sand turbulence simulation on the propellers reduced the open water efficiency and propulsive coefficient by 10 and 9 percent respectively, producing an unrealistically low efficiency [21].

The INSEAN/University of Iowa experiments were conducted to further define the complex flow around a surface combatant hull and contribute to the database of surface-ship model scale propulsion for CFD code validation. The INSEAN model had no appendages apart from the bow SONAR dome and skeg, which is reflected in the overall increase of effective resistance shown in Figure 28.Displacement and draft conditions were the same as the NSWC-CD conditions. Across the range of overlapping Froude numbers, the NSWC-CD data with the appendages showed an average of 30.5% increase in effective resistance of the INSEAN data that did not include the hull appendages.

2.2.4.1 Motor Sizing and Selection

The sizing and selection of the propulsion motors began with the scaled resistance data and the characteristics of the DTMB 4381 propeller. In determining the power required to propel the ship, several hydrodynamic interactions must be taken into account. The first is the action of the hull on the propeller inflow due to the frictional drag of the hull, the streamline flow convergence around the stern, and the velocity of the hull generated waves. This combination of interactions is accounted for in the Taylor wake fraction (w) and is applied to transform the ship velocity, V, to the advance velocity, V_a.

$$V_a = V(1 - w) \tag{21}$$

The second interaction is the difference in resistance between a towed hull and one being self-propelled. The area of high pressure over the stern effectively reduces the resistance of the hull when being towed. In the self-propelled configuration, the pressure over the stern is reduced because of the acceleration of the wake through the stern region, thereby increasing the effective resistance of the ship. This effect is accounted for by a thrust-reduction factor, *t*, where

$$t = \frac{T - R_T}{T} \text{ or } R_T = (1 - t)T \tag{22}$$

Here, R_T is the resistance when towed and T is the self-propelled resistance. Because tow tank testing was not available to measure these values and there was no record of them in the literature for the DTMB 5415 hull, widely accepted nominal values of 0.2 were used for both. Together, the wake and thrust deduction factors can be used to determine the total hull efficiency, η_{hull}.

$$\eta_{hull} = \frac{1 - t}{1 - w} \tag{23}$$

Once the fractions were determined, the towed resistance of the hull was interpolated from the available INSEAN resistance data using Froude scaling. The frictional resistance of the model,C_{Fm}, a function of Reynolds number, Re_m, was calculated using the 1957 International Towing Tank Conference (ITTC) curve. The total resistance coefficient and dimensional resistance for the model was calculated as shown below where S_m is the model's wetted surface area.

$$C_{Fm} = \frac{0.075}{(log_{10}(Re_m) - 2)^2} \tag{24}$$

$$C_{Tm} = C_{Fm} + C_{Rm} \tag{25}$$

$$R_{Tm} = 0.5\rho C_{Tm} {V_m}^2 S_m \tag{26}$$

The final required power was determined by tracking the power required by the propeller to the brake power delivered to the motor when operating at the maximum intended speed (31 knots full scale and 9.25 ft/sec at model scale).

$$\text{Effective towing power, } P_e = R_{Tm} V_m \tag{27}$$

$$\text{Required hull thrust power per propeller, } P_t = \frac{P_e}{k_p \eta_{hull}} \tag{28}$$

$$\text{Required open water propeller power, } P_o = \frac{P_t}{\eta_{open}} \tag{29}$$

$$\text{Reqiured propeller power, } P_p = \frac{P_o}{\eta_{relrot}} \tag{30}$$

$$\text{Required shaft power, } P_s = \frac{P_p}{\eta_{shaft}} = P_{brake} \tag{31}$$

$$\text{Shaft speed, } n = \frac{V_a}{J_s D} \tag{32}$$

$$\text{Required torque per motor, } Q_m = \frac{P_b}{2\pi n} \tag{33}$$

The resulting torque per shaft at the maximum design speed of 9.25 ft/sec was 1.88 N-m, or 1.39 ft-lbs. Brushless direct current (DC) permanent magnet servo motors were decided as the best propulsion power option because of their high degree of controllability, reliability and feedback, which will be needed while testing the crashback maneuver and measuring the power regeneration. Also referred to as an alternating current (AC) synchronous motor, the brushless DC motor is a three phase synchronous AC motor with a position transducer built into the motor housing to communicate the shaft position to the drive amplifier to control current commutation in the motor windings. Two Kollmorgen AKM-41E's were selected because of their maximum rated continuous torque and power requirements. The motors operate off of 120 VAC, have a max speed of 2,430 RPM and a continuous torque of 2.02 N-m, or 1.49 ft-lbs, providing a 7.2% margin for the maximum operating condition. The motor torque constant, k_t, is 0.71 N-m/A_{rms}.

The motors are driven by two120 VAC Kollmorgen AKD P00-306 drives. Because the motor is overmatched and provides a high degree of programmability, tuning the motor torque response to increases in demanded thrust while maneuvering is a fairly simple procedure. A simplified model for determining the dynamics of a permanent magnet DC motor for use in a ship maneuvering model is provided in [22].

During the crashback maneuver, the propulsion motor is ordered to go from all ahead full to all back full. When this occurs, the motor temporarily becomes a generator as the inertia of the drive train continues to turn in the standard ahead direction. In addition to the dry mass moment of inertia of the propeller (I_P) and the shafting (I_S), hydrodynamic inertia exists due to the viscous nature of water and results in entrained water around the propeller disc. This added inertia (I_E) can be on the same order of magnitude or greater than the dry propeller inertia. The rotating fluid has a different effect across the radius of each blade because of the greater distance the fluid is displaced at the tip versus the root. Several methods exist for early stage design estimation of this property, including the Parson method, the Schwanecke method, and the Burrill method [23]. All rely heavily on empirical testing and coefficients derived from a standard series of propellers and don't capture the distribution of the propeller parameters over the blade radii. MacPherson et al. (2007) found that pitch distribution and blade outline (i.e. the chord distribution) both have significant influence on I_E and developed a semi-empirical blade element integration method. The method assumes that the torsional wetted inertia, I_E, is proportional to the profile area of the blade element in rotation, as shown in Figure 29.

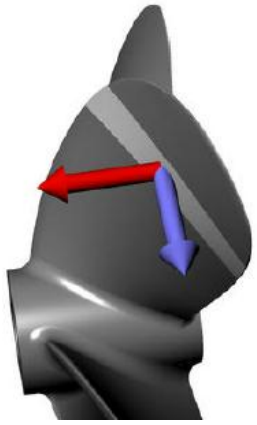

FIGURE 29-BLADE ELEMENT (REPRODUCED FROM [23])

I_E is calculated as:

$$I_E = K_I \frac{\pi \rho Z}{4} \int_{r_{Hub}}^{r_{Tip}} (r \cos \varphi)^2 \, dr \tag{34}$$

where K_I is a semi-empirical wetted inertia factor. Historical K_I factors provided by Burrill were found by MacPherson to over-predict the wetted inertia by as much as 10% [23]. The raw Burrill data was reanalyzed and during the course of the analysis, it was determined that the pitch to diameter ratio contributed to K_I. Once a $^{P}/_{D}$ correction factor was determined, the same test data was analyzed and found to match Burrill's experimental testing [23]. The validated MacPherson et al. method for calculation K_I is:

$$K_I = \frac{1 + 12.47 \frac{EAR}{Z} - 16.7 \left(\frac{EAR}{Z}\right)^2}{\left(22.58 \frac{EAR}{Z}\right)\left(1.14 - \frac{0.161}{P/D}\right)} \tag{35}$$

This method was applied to the model's modified DTMB 4381 propellers and the results are shown in Table 5-Model propeller inertia along with the propeller's dry inertia determined in SolidWorks. Initial modeling using a Kollmorgen software tool concluded that regenerative resistors would not be needed for the drives because of the internal capacitance built it. Should open water testing prove otherwise or new propellers with greater inertia be installed, external Kollmorgen regenerative resistors can easily be integrated into the drive through a simple connection interface.

TABLE 5-MODEL PROPELLER INERTIA

$I_{Entrained\ Water}$	4.06E-04	$\left[{}^{kg}/_{m^2}\right]$
$I_{Dry\ Propeller}$	2.00E-04	$\left[{}^{kg}/_{m^2}\right]$
$I_{Shafting}$	2.34E-05	$\left[{}^{kg}/_{m^2}\right]$
I_{Total} (I_{xx})	6.29E-04	$\left[{}^{kg}/_{m^2}\right]$

2.2.5 Control

Control of the servo motors and stepper motors is provided by a Baldor Motion NextMove e100. This particular controller was selected, one because of its existing software support and ActiveX integration and because of its TCP/IP networking capability. The e100 provides real-time control of up to three servo axes and four stepper axes over an Ethernet network. Using the Baldor Mint Workbench software and the Mint Motion programming language, a motion control code was written to couple the propulsion servo motors and the rudder stepper motors. The code is provided in Appendix D. Initially, a slave-master relationship was created between the respective stepper and motor drives; however, this configuration inherently leads to delays in execution. This unwanted effect was overcome by creating a virtual servo axis and a virtual stepper axis to act as primary master axes for the real drives and motors. Once commanded to move, the slaves follow the virtual masters in sync. Because the servo and stepper motors have selectable step resolutions and encoder pulse outputs, scale factors were used within the controller code to transform the operating units of the servo motors to revolutions per minute (RPM) and the stepper motors to whole degrees. There are two closed loop control schemes, a proportional integral (PI) controller and a proportional integral derivative (PID) controller. First, the gains of the velocity loop of the AKD motor drives (the PI controller) were tuned using the software's generic Slider Tuning interface. Additional information on the load inertia can be entered to achieve better system response. The gains of the Baldor e100's position and velocity loops (the PID controller) were then manually tuned to limit the overshoot of the final shaft speed. The system must be tuned whenever changes are made to the load, e.g. the shafting or propeller. The IMS MDrive stepper motors do not have encoders, and therefore the scale factor was determined directly by the microstep resolution. The Kollmorgen AKDs employ the Smart Feedback Device and an encoder emulator that allow for custom configuration of quadrature counts per revolution. The initial parameters are captured in the Startup Block of the Mint motion code in Appendix D. The scale factors and resolutions are shown in Table 6.

TABLE 6-SERVO AND STEPPER MOTOR SCALE FACTORS AND RESOLUTION

Drive	Configured microstep resolution [steps/rev]	Encoder counts per revolution [quad counts/rev]	Scale Factor
Kollmorgen AKD (servo)	-	14,400	40 [quad counts/degree]
IMS MDrive (stepper)	36,000	-	100 [μsteps/degree]

The host PC communicates with the onboard controller through a standard TCP/IP 802.11 n/g/b router stationed onboard the model. The range of the wireless network was extended by using omni-directional, outdoor, 8dBi, 2.4 GHz antennas on both the model and the shore wireless adapters. Theoretically, this increases the communications range up to 700 yards in a line of sight condition.

2.2.6 Onboard Sensors

Precise vessel position and attitude time history was desired for experimentation. To achieve this, an integrated accelerometer, gyro and GPS was necessary that would provide pitch, yaw, roll, velocity and global positioning. The MicroStrain 3DM-GX3-45 was selected. The sensor is a GPS-aided inertial navigation system (GPS/INS) with an Attitude and Heading Reference Unit (AHRS), GPS receiver, and an onboard processor running an Extended Kahlman Filter (EKF) that combines the sensor outputs into a single solution. The AHRS consists of the standard sensors found in an Inertial Measurement Unit (IMU) as well as an algorithm to resolve the sensor data into roll, pitch, and yaw/heading. The inertial sensors include gyroscopes, accelerometers and magnetometers. While an accelerometer is sufficient for short duration attitude determination, it is not adequate for low frequency maneuvers such as a steady turn. The algorithm assumes that the acceleration due to Earth's gravity dominates the acceleration vector and is changed only by short, transient linear accelerations of the vehicle. During a long duration, low frequency maneuver, such as a steady turn, the pitch and roll angles reported would be wrong due to the initial assumption. Incorporating a gyro alleviates this problem, and allows for precise attitude determination during low frequency maneuvering. The processor runs a loosely-coupled EKF, where the inertial sensors in the AHRS supply the state estimation at a rate of 100 Hz and the GPS provides position and velocity measurements to update the estimations at 4 Hz. The magnetometer corrects heading misalignments that occur during low frequency

maneuvering. Data from the IMU is stored via an onboard microcontroller as well as transmitted to the controller over the TCP/IP wireless network for test monitoring.

2.3 Performance Characteristics

2.3.1 Open Water Trials

Initial maneuvering tests will be conducted to tune the propulsion system and measure the models maneuvering characteristics. This is important both to fully characterize the model and test all the onboard components. The ITTC provides recommend procedures and guidelines for the trials, which should include:

1. Straight line speed run for motor RPM tuning
2. Turning circle test with hard over rudder (35° port and starboard)
3. Pull-out test with rudder from hard over to centerline until yaw reaches zero
4. Zig-zag test (10°/10°, 20°/20°, or modified)
5. Spiral test (steady turning test at 5°, 10°, 15°, 20°, and 25°.)

Although it would seem that a full astern stopping test would be desired, it is not typically conducted because of the lack of scaling in the viscous resistance.

2.3.2 Testing Conditions Specific to Future Research

The model will have two immediate applications that will require special consideration of the mass properties and motor tuning parameters. The first case is that of imaging the flow over the propellers and rudders during the crashback maneuver. During the test, the model will be moving only in surge and the rudders will be kept at zero degrees (centerline) and will not be producing any turning moments on the hull. If it is assumed that the ship does not translate in the y-direction or rotate about the z-axis, then the motion of the ship is governed solely by the decoupled, non-linear surge equation of motion shown in Equation 36 in the standard SNAME notation. This assumption is supported by the dual propellers operating in opposing directions, effectively cancelling out any torque that would generate a moment on the hull. In reality, however, the complex interactions of the propellers and hull, the unbalanced thrust of the propellers, and the existence of any external forces will produce a turning moment on the hull.

$$
\begin{aligned}
&m(\dot{u} - rv - r^2 x_G) \\
&= X_o + X_{\dot{u}}\dot{u} + X_u u + X_{uu}u^2 + X_{uuu}u^3 + X_{vv}v^2 + X_{rr}r^2 \\
&+ X_{vvu}v^2 u + X_{rru}r^2 u + X_{vr}vr + X_{vru}vru + External\ Forces
\end{aligned}
\tag{36}
$$

When linearized, all of the non-surge cross-terms drop out and produce

$$
\dot{u}(m - X_{\dot{u}}) - X_u u = External\ Forces \tag{37}
$$

Under the assumption of unidirectional motion, the parameters governing the deceleration are the ship's resistance as a function of velocity, the reverse propeller thrust, the inertia of the ship's mass, *m*, and the longitudinal added mass, $X_{\dot{u}}$. To achieve similitude in the model's response, therefore, the mass should be properly scaled by λ^3 and the nondimensional added mass, $X_{\dot{u}}{}'$, should remain constant. This second condition is inherently taken care of by the geometric similitude between the model and full scale. Additionally, the dynamics of the propulsion system, specifically the rate of change of the propeller thrust, should be matched. The rate of change of thrust has historically been assumed as linear for crashback [13]. Time scales as $\lambda^{1/2}$, which means that for λ=30, events for the model should take only 18.2% of the time of the full scale and force scales as λ^3, or 3.70 x 10^{-5} times the full scale. Using these scaling factors, a linear thrust profile can be generated and the corresponding propeller RPM can be determined in order to fully simulate a time-resolved crashback event.

The second case is that of decreasing the speed loss during maneuvers through active control of vortex shedding. During turning maneuvers, the motion of the ship is governed by the surge equation provided above as well as the coupled sway-yaw equations shown below.

$$
\begin{aligned}
m(\dot{v} - ru - \dot{r}x_G) &= Y_{\dot{v}}\dot{v} + Y_{\dot{r}}\dot{r} + Y_v v + Y_{vvv}v^3 + Y_r r + Y_{rrr}r^3 + Y_{vrr}vr^2 + \\
&Y_{vu}vu + Y_{ru}ru + Y_{vuu}vu^2 + Y_{rvv}rv^2 + Y_{ruu}ru^2 + External\ Forces + \\
&Actuator \text{ Terms}
\end{aligned}
\tag{38}
$$

$$
\begin{aligned}
I_{zz}\dot{r} + mx_G(\dot{v} + ru) &= N_{\dot{v}}\dot{v} + N_{\dot{r}}\dot{r} + N_v v + N_{vvv}v^3 + N_r r + N_{rrr}r^3 + \\
&N_{vrr}vr^2 + N_{vu}vu + N_{ru}ru + N_{vuu}vu^2 + N_{rvv}rv^2 + N_{ruu}ru^2 + \\
&External\ Moments + Actuator \text{ Terms}
\end{aligned}
\tag{39}
$$

According to these equations of motion, I_{zz}, m, and x_G must all be properly scaled to maintain similitude. As in the crashback scenario, the propulsion dynamics must be properly matched between the model and full-scale. Prior to initiating a maneuver, when the ship is moving in a straight line at constant speed, the balance of propeller thrust, *T*, and total hull resistance, *R*, is modeled as

$$X = T(1-t) - R = 0 \tag{40}$$

However, as soon as a turn it initiated, the equilibrium no longer exists as *R* and *t*, thrust deduction, are a function of ship speed and *T* is a function of both ship speed and the type of propulsion plant. Diesel driven shafts can be assumed as constant torque machines and shaft RPM will subsequently decrease as more torque is required to maintain a specific shaft speed. Induction motors, being constant speed machines, maintain the propeller speed, and hence thrust, regardless of the increase in torque demand [20]. Therefore, depending on the type of propulsion plant being modeled, the servo motors should be set up for either constant velocity or constant torque.

3 FUTURE EXPERIMENTAL TESTING

3.1 Crashback Transients

With the construction of the DDG 1000 class of ships, the US Navy has committed itself to fully integrated power systems where both the propulsion and ship service loads are supplied from a single electrical architecture. Propulsion power is provided through large electric motors rather than a directly coupled prime mover. Although this method optimizes the use of the ship's prime movers, the direct connection of the propulsion machinery, weapons systems and hotel loads to one electrical network presents a complex power management problem. An extreme case exists when a ship with a fixed-pitch propeller conducts the crashback maneuver. During this phase, the propulsion motor temporarily acts as a generator, creating excess power that must be stored or consumed. The effects of these power transients on the ship's distribution system are not fully understood. The scale model provides a platform to accurately replicate the crashback condition in similar operating conditions with full scale naval vessels and monitor the effects of vessel propulsion demands on a notional integrated electrical distribution system.

3.2 Increasing slender body turning efficiency

Ocean going streamlined bodies, i.e. ships, are subject to hull flow separation while turning. The separation and subsequent vortical flows can add a substantial amount of drag and drastically reduce the turning efficiency of the vessel, measured by the turning radius and velocity lost in the turn. Sakamoto (2009) applied CFD methods to characterize the flow around a DTMB 5415 hull and validated it with experimental planar motion mechanism tests. The report documents three origins for flow separation and vortex generation along the length of the hull with the most dominant being the sonar dome (SD), the bilge keels (BK), and the after keel (AK) as shown in Figure 30.

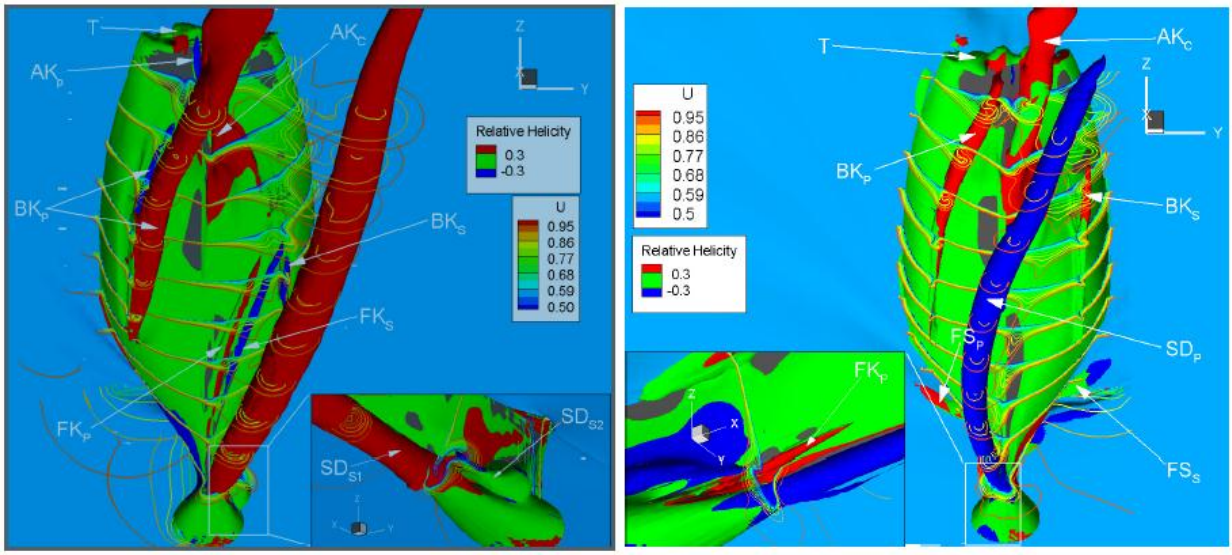

FIGURE 30-VORTICAL FLOWS AROUND THE DTMB 5415 HULL IN STEADY MANEUVER AT A STATIC DRIFT ANGLE = 10° (LEFT) AND STEADY TURN (RIGHT) (REPRODUCED FROM[17])

Active flow separation control has been shown to reduce hydrodynamic separation drag and oscillating lift forces by adding momentum to the slow moving boundary layer flow along the hull. The addition of momentum delays the onset of flow separation and reduces the overall hydrodynamic drag. With any active control system, it is paramount that the power required to operate the system is less than that lost without the system. In the case of reducing the hydrodynamic drag, the increase in power from the viscous drag (friction drag) of the apparatus

and the power to operate the machinery must be less than that lost in the normal operating condition. Current research modeling the main flow body as a stationary cylinder and employing two rotating cylinders placed at 120° to the oncoming flow has shown promising reductions in both velocity fluctuations and the wake momentum deficit [24]. Should the research reach a point at which scale model testing is required, the 1/30th scale, free-running model will provide a suitable platform.

4 CONLCUSIONS

4.1 Future Work and Lessons Learned

The 1/30th scale, free-running DTMB 5415 model designed and built is a great asset to the MIT Ocean Engineering Department. The AKM servo motors and onboard controller makes generation of specific motion profiles a trivial matter, accessible to any student and its onboard IMU provides accurate, time stamped data for precise motion monitoring. The model will provide a flexible test platform for years of research and experimentation, with the immediate areas of interest including visualization of crashback propeller loading, improving slender body turning efficiencies, and electrical plant implications of the crashback maneuver. All of these are of current interest to the US Navy. While the majority of the scaling laws outlined in Section 1.1.3 were met, several of the mass similitude guidelines require further attention and tuning should it be desired that the accurately reflect the maneuvering of full scale DTMB 5415.

WORKS CITED

[1] S. Jessup, S. Swithenbank and A. Etebari, "Measurement of Crashback Loads on a Blade of Propeller 4381 in an Open and Ducted Confirguration in the 36-inch Water Tunnel," NSWC-Carderock, Bethesda, 2008.

[2] S. Jessup, C. Chesnakas, M. Donnelly, S. Black and J. Park, "Propeller Performance at Extreme Off Design Conditions," in *25th Symposium on Naval Hydrodynamics*, St. John's, Newfoundland and Labrador, 2004.

[3] S. Jessup, D. Fry and M. Donelly, "Unsteady Propeller Performance in Crashback Conditions With and Without a Duct," Naval Surface Warfare Center Carderock Division, West Bethesda, 2006.

[4] B. Chen and F. Stern, "Computational Fluid Dynamics of Four-Quadrant Marine-Propulsor Flow," *Journal of Ship Research*, vol. 43, no. 4, pp. 218-228, 1999.

[5] M. Vysohlid and K. Mahesh, "Understanding Crashback in Marine Propellers Using an Unsteady Actuator Disk Model," University of Monnesota, Minneapolis, 2007.

[6] *Discussions with Brenden Epps.* [Interview]. January 2012.

[7] "IIHR - Hydroscience & Engineering Ship Hydrodynamics Website," University of Iowa, March 2010. [Online]. Available: http://old.iihr.uiowa.edu/~shiphydro/index.htm. [Accessed December 2011].

[8] J.-H. Chen and C.-C. Chang, "A moving PIV system for ship model test in a towing tank," Elsevier, Taiwan, 2005.

[9] J. Belden, "Synthetic Aperature Imaging for Three Dimensional Resolution of Fluid Flows," Massachusetts Institute of Technology, Cambridge, 2011.

[10] ITTC, "ITTC Recommended Procedures and Guidelines: Testing and Extrapolation Methods-Maneuverability-Free Running Model Tests," 2008. [Online]. Available: http://ittc.sname.org/CD%202011/ITTC%20Contents.pdf. [Accessed 21 March 2012].

[11] ITTC, "Recommended Procedures and Guidelines-Ship Models," 2011. [Online]. Available: http://ittc.sname.org/CD%202011/ITTC%20Contents.pdf. [Accessed 21 March 2012].

[12] ITTC Resistance Committee, "Final Report and Recommendations to the 26th ITTC," SNAME, Rio de Janeiro, 2011.

[13] E. V. Lewis, "Controllability," in *Principles of Naval Architecture: Motions in Waves and Controllability, Volume III*, Jersey City, The Society of Naval Architects and Marine Engineers, 1989, pp. 215-217.

[14] L. Lazaukas, "Resistance and Squat of Surface Combatant DTMB 5415: Experiments and Predictions," Cyberiad, 2009.

[15] A. Olivieri, F. Pistani, A. Avanzini, F. Stern and R. Penna, "Towing Tank Experiments of Resistance, Sinkage, and Trim, Boundary Layer, Wake, and Free Surface Flow around a Naval Combatant INSEAN 2340 Model," Istituto Nazionale per Studi ed Esperienze di Architettura Navale, Roma, 2001.

[16] N. Sakamoto, "URANS and DES Simulations of Static and Dynamic Maneuvering for Surface Combatant," University of Iowa, Iowa City, 2009.

[17] H. Yoon, "Phase-Averaged Stereo-PIV Flow Field and Force/Moment/Motion Measurements for Surface Combatant in PMM Maneuvers," University of Iowa, Iowa City, 2009.

[18] SIMMAN, "Workshop on Verification and validation of Ship Manoeuvering Simulation Methods," 2008. [Online]. Available: http://www.simman2008.dk/5415/5415_geometry.htm. [Accessed 15 January 2012].

[19] C. Chesnakas and T. Ratcliffe, "Propeller Flow Field Mapping of Model 5415 using 3-Component Laser Doppler Velocimetry," Naval Surface Warfare Center, Carderock Division, West Bethesda, 2005.

[20] E. V. Lewis, "Propulsion," in *Principles of Naval Architecture Volume II: Resistance, Propulsion and Vibration*, Jersey city, SNAME, 1988, pp. 153-155.

[21] G. Borda, "Resistance, Powering and Optimum Rudder Angle Experiments on a 465.9 foot (142m) Guided Missile Destroyer (DDG-51) Represented by Model 5415-1 and Fixed Pitch Propellers 4876 and 4877," David W. Taylor Naval Ship Research and Development Center, Bethesda, 1984.

[22] J. W. Stettler, Steady and Unsteady Dynamics of an Azimuthing Podded Propulsor Related to Vehicle Maneruvering, Cambridge: Massachusetts Institute of Technology, 2004.

[23] D. M. MacPherson, V. R. Puleo and M. B. Packard, "Estimation of Entrained Water Added Mass Properties for Vibration Analysis," HydroComp, Inc., 2007.

[24] *Discussions with James Schulmeister.* [Interview]. March 2012.

[25] N. Berchiche, "Numerical predictions of crashback propeller flow and loadings," Chaimers University of Technology, Gothenburg, Sweden.

[26] S.-J. Tsai, B. Hopkins and R. Stenson, "Comparison of Powering Performance Between DDG-51 and Conventional Combatant Hull Forms," *Naval Engineers Journal*, pp. 88-99, 1994.

[27] M. S. Triantafyllou and F. S. Hover, *Maneuvering and Control of Marine Vehicles*, Cambridge: MIT, 2002.

[28] L.-P. M. Menard, "Prediction of Performance and Maneuvering Dynamics for Marine Vehicles Applied to DDG-1000," Massachusetts Institute of Technology, Cambridge, 2012.

[29] H. K. Woud and D. Stapersma, Design of Propulsion and Electric Power Generation Systems, 1st ed., London: Institute of Marine Engineering, Science and Technology, 2002.

[30] P. A. Chang III, M. Ebert, K. Mahesh, H. Jang, Y. L. Young, Z. Liu and M. Shearer, "Propeller Forces And Structural Response Due To Crashback," 27th Symposium on Naval Hydrodynamics, Seoul, 2008.

[31] S. Black and S. Swithenbank, "Analysis of Crasback Forces Compared with Experimental Results," NSWC-Carderock, Bethesda, 2009.

[32] M. Montero, S. Roundy, D. Odell, S.-H. Ahn and P. K. Wright, "Material Characterization of Fused Deposition Modeling (FDM) ABS by Designed Experiments," 2001.

[33] J. N. Newman, Marine Hydrodynamics, Cambridge: MIT Press, 1977.

5 APPENDICES

Appendix A-Propeller 4381 Four Quadrant Data

Ahead				Astern				Crashback				Crashahead		
J	KT	KQ		J	KT	KQ		J	KT	KQ		J	KT	KQ
0	0.578	0.952		0	-0.43	-0.89		0	-0.43	-0.89		0	0.578	0.952
0.05	0.56	0.927		0.05	-0.424	-0.872		-0.05	-0.439	-0.904		-0.05	0.586	0.961
0.1	0.542	0.9		0.1	-0.413	-0.851		-0.1	-0.442	-0.913		-0.1	0.582	0.96
0.15	0.524	0.875		0.15	-0.402	-0.824		-0.15	-0.449	-0.921		-0.15	0.578	0.949
0.2	0.506	0.846		0.2	-0.386	-0.795		-0.2	-0.45	-0.924		-0.2	0.562	0.935
0.25	0.487	0.818		0.25	-0.371	-0.764		-0.25	-0.449	-0.923		-0.25	0.548	0.914
0.3	0.469	0.789		0.3	-0.353	-0.731		-0.3	-0.443	-0.915		-0.3	0.53	0.892
0.35	0.448	0.759		0.35	-0.335	-0.695		-0.35	-0.43	-0.888		-0.35	0.51	0.869
0.4	0.428	0.73		0.4	-0.315	-0.659		-0.4	-0.401	-0.818		-0.4	0.485	0.836
0.45	0.404	0.698		0.45	-0.291	-0.619		-0.45	-0.351	-0.714		-0.45	0.452	0.798
0.5	0.383	0.668		0.5	-0.272	-0.579		-0.5	-0.331	-0.671		-0.5	0.419	0.75
0.55	0.362	0.637		0.55	-0.247	-0.538		-0.55	-0.35	-0.692		-0.55	0.411	0.736
0.6	0.34	0.602		0.6	-0.224	-0.492		-0.6	-0.392	-0.763		-0.6	0.435	0.76
0.65	0.318	0.577		0.65	-0.198	-0.448		-0.65	-0.448	-0.85		-0.65	0.488	0.842
0.7	0.295	0.545		0.7	-0.174	-0.4		-0.7	-0.503	-0.936		-0.7	0.543	0.931
0.75	0.273	0.513		0.75	-0.148	-0.353		-0.75	-0.562	-1.025		-0.75	0.604	1.022
0.8	0.25	0.481		0.8	-0.121	-0.303		-0.8	-0.618	-1.11		-0.8	0.662	1.104
0.85	0.227	0.448		0.85	-0.094	-0.255		-0.85	-0.675	-1.198		-0.85	0.719	1.194
0.9	0.202	0.411		0.9	-0.067	-0.203		-0.9	-0.732	-1.285		-0.9	0.779	1.276
0.95	0.189	0.374		0.95	-0.039	-0.149		-0.95	-0.79	-1.37		-0.95	0.836	1.36
1	0.152	0.335		1	-0.012	-0.099		-1	-0.846	-1.457		-1	0.898	1.446
1.052632	0.13	0.291		1.022495	0	-0.076		-1.05263	-0.907	-1.546		-1.05263	0.96	1.538
1.111111	0.104	0.242		1.052632	0.019	-0.048		-1.11111	-0.972	-1.645		-1.11111	1.028	1.642
1.176471	0.069	0.183		1.111111	0.049	0.011		-1.17647	-1.044	-1.761		-1.17647	1.105	1.751
1.25	0.021	0.105		1.176471	0.088	0.081		-1.25	-1.129	-1.898		-1.25	1.195	1.883
1.28041	0	0.073		1.25	0.135	0.16		-1.33333	-1.23	-2.049		-1.33333	1.297	2.041
1.333333	-0.035	0.002		1.333333	0.19	0.259		-1.42857	-1.346	-2.227		-1.42857	1.414	2.227
1.428571	-0.118	-0.131		1.428571	0.263	0.391		-1.53846	-1.477	-2.427		-1.53846	1.555	2.457
1.538462	-0.218	-0.299		1.538462	0.36	0.563		-1.66667	-1.647	-2.688		-1.66667	1.724	2.747
1.666667	-0.336	-0.505		1.666667	0.481	0.792		-1.81818	-1.862	-3.049		-1.81818	1.957	3.147
1.818182	-0.485	-0.77		1.818182	0.664	1.142		-2	-2.141	-3.509		-2	2.252	3.623
2	-0.702	-1.133		2	0.928	1.603		-2.22222	-2.519	-4.167		-2.22222	2.66	4.329
2.222222	-1	-1.661		2.222222	1.225	2.193		-2.5	-3.058	-5.208		-2.5	3.226	5.263
2.5	-1.443	-2.41		2.5	1.681	2.994		-2.85714	-3.832	-6.494		-2.85714	4.065	6.803
2.857143	-2.123	-3.597		2.857143	2.421	4.367		-3.33333	-5	-8.403		-3.33333	5.464	9.434
3.333333	-3.175	-5.435		3.333333	3.636	6.667		-4	-6.775	-11.442		-4	7.262	12.987
4	-4.85	-8.17		4	5.656	10.941		-5	-9.141	-15.337		-5	9.97	17.483
5	-8.475	-14.144		5	9.05	17.699		-6.66667	-14.144	-23.753		-6.66667	15.198	26.738
6.666667	-16.835	-27.548		6.666667	17.271	32.573		-10	-29.499	-49.02		-10	30.96	53.763
10	-37.453	-62.5		10	40.65	77.519		-20	-83.333	-156.25		-20	114.943	192.308
20	-102.041	-212.766		20	120.482	263.158								

Appendix B-Modified Propeller 4381 Geometry

```
% ------------------------------------------------------------------------
% Propeller geometry definition
% ------------------------------------------------------------------------
% ------------------------------------------- Blade 2D section properties
Meanline   = 'NACA a=0.8';              % Meanline type
Thickness  = 'NACA66 (DTRC Modified)';  % Thickness form
% alphaI     = 1.54;        % [deg] ideal angle of attack  (should match with Meanline type)
% CLI        = 1.0;         % [ ],  ideal lift coefficient (should match with Meanline type)

XR           = [0.2000    0.3000    0.4000    0.5000    0.6000    0.7000    0.8000    0.9000
0.9500    0.9800    0.9900    1.0000];  % radius / propeller radius
XCoD         = [0.1740    0.2280    0.2750    0.3130    0.3380    0.3480    0.3340    0.2810
0.2190    0.1530    0.1150    0.0010];  % chord / diameter  (12/6/2011 NOTE: finite chord at tip:
0.0010)
XPoD         = [1.2600    1.3500    1.3600    1.3400    1.2800    1.2100    1.1400    1.0700
1.0300    1.0100    1.0100    1.0000]; % pitch / diameter
f0oc0        = [0.0312    0.0369    0.0348    0.0307    0.0244    0.0189    0.0147    0.0122
0.0133    0.0164    0.0211    0.0280]; % max section camber    / chord
% t0oc0        = [0.2500    0.1560    0.1070    0.0770    0.0570    0.0420    0.0310    0.0240
0.0260    0.0370    0.0500    0.0700]; % max section thickness / chord
skew0      = zeros(size(XR));   % skew
rake0      = zeros(size(XR));   % rake

theta0     = atand(XPoD./(pi*XR));      % Nose-tail pitch angle, [deg]

% t0oD0 = t0oc0 .* XCoD;

Mx = length(XR);

% ---------------------------------------- Define other geometry parameters
Hub_flag = 1;      % 0 == no hub, 1 == hub
Z    = 5;            % blades

D    = 6.8000 * 0.0254;  % == 0.1727 m, propeller diameter  (we used 0.1665 m on 110721)
Dhub = 0.2*D;
% ------------------------------------------------------------------------

Rhub_oR = XR(1);

% ------------------------------------------------
% 12/6/2011  Blade thickness profile (from ESRDC CRP propeller project)
t0hub = 0.2958*0.0254; % [m] == 0.450 inch (for model), max thickness at hub section
t0tip = 0.150*0.0254; % [m] == 0.150 inch (for model), max thickness at tip section
t0tpm = 0.080*0.0254; % [m] == 0.080 inch (for model), modified tip thickness
XRmax = 0.80;              % maximum XR for which thickness reduction is less than 1%
TTRF  = t0tpm/t0tip;       % Tip Thickness Reduction Factor == modified thickness at tip /
baseline thickness at tip
HTTR  = t0hub/t0tip;       % Hub-Tip Thickness Ratio        == t0(hub) / t0(tip)
t0oc0 = t0tip*(HTTR - (HTTR-1).*(XR-Rhub_oR)/(1-Rhub_oR))./(XCoD*D) .* (1-(1-TTRF)*exp(-4.6*(1-
XR)/(1-XRmax)));
t0oD0 = t0oc0.*XCoD;
t0    = t0oD0*D;

% original 4381 data from above
t0oc0_4381  = [0.2500    0.1560    0.1070    0.0770    0.0570    0.0420    0.0310    0.0240
0.0260    0.0370    0.0500    0.0700]; % max section thickness / chord
```

Appendix C-IMS MDrive23 Stepper Setup Code

```
S7 = 33,0  'IO7 = step input, active LOW
S8 = 33,0  'IO8 = direction input,active LOW

Ms = 180
Cr = 1.000
Cm = 1

S
```

Appendix D-Balder e100 Control Code for MINT Workbench

```
'Motor controller for MIT Sea Grant DTMB 5415 1/30th scale model.

'Written by Dave Cope
'Last revision 5/1/2012

'READ BEFORE USE!!!
'This program allows the user to control the propulsion servo motors and the
rudder stepper motors either
'using the Command window or using the Comms array in the Mint WorkBench.
Both the
'AKD servo drives (using Kollmorgen WorkBench) and the IMS stepper drives
(using IMS Terminal) have been configured to work with this and must be
'reconfigured if any factors are altered.  For easy configuration, the drives
are ethernet enabled and the IP
'addresses are listed below. As it is set up now, the Port motor turns
counter-clockwise and the
'Starboard turns clockwise.

'This program is meant to be used with Device Configuration File
DTMB5415_Actual.dcf

'Servo IP Address
'Port AKD Drive       - 192.168.0.2
'Starboard AKD Drive  - 192.168.0.1

'Stepper IP Adress
'Both Drives          -192.168.33.1

'Baldor Controller IP - 192.168.100.1 This is set by the rotary switches on
the controller in Hex-decimal format see e100 manual 5-2-4

'TP-Link Wireless Adapter Settings
'IP Address           -192.168.100.241
'Subnet Mask          -255.255.255.0



'Notes and things to add
  '-Need to include eration OF both the servos And steppers
  '-Use the 'STOP' command to stop all motion
  '-Use the 'ABORT' command to shut down the program and stop the drives and
motors.
  '-After using 'ABORT' the program must be restarted to enable the drives
  '-Wireless ethernet communication loss shutdown

'-------------------------------------------------------------------------
------------------
 Auto   'this automatically initiates the program upon startup

' Defines Master Axes
Define ShaftMaster = 0    'master axis # for shaft
Define RudderMaster = 3   'master axis # for rudders
```

```
' Defines for Comms Array usage
Define ShaftSpeed   = 1
Define RudderAngle  = 2
' Enable both the Servo Propeller Drives and the Rudder Stepper Drives
CANCELALL

DRIVEENABLEOUTPUT(1)=12
DRIVEENABLEOUTPUT(2)=12

DRIVEENABLE(0) = 1   'Propller virtual master axis
DRIVEENABLE(1) = 1   'Propeller port servo
DRIVEENABLE(2) = 1   'Propeller starboard servo
DRIVEENABLE(3) = 1   'Rudder virtual master axis
DRIVEENABLE(4) = 1   'Rudder port stepper
DRIVEENABLE(5) = 1   'Rudder starboard stepper
'-------------------------------------------------------------------
' RUDDER SETUP PARAMETERS

'Rudder slew rate.  This stepper slew speed is determined from a non-
dimensional rudder slew rate discussed in my thesis multiplied by 2 because
of the gear ratio on he acutal rudders.  Rudders should slew at 49.3 [deg/s].
SPEED(3) = 98.6       '[degrees/second]

'Need to set to actual channels on the drive, not axes
SCALEFACTOR(3) = 100
SCALEFACTOR(4) = 100
SCALEFACTOR(5) = 100

'Rudder angle limits
SOFTLIMITMODE(3) = _emCALL_HANDLER
SOFTLIMITFORWARD(3)= 36
SOFTLIMITREVERSE(3)= -36

'Move trigger mode for rudders
TRIGGERMODE(3) = _trAUTO  'Rudders will move upon entering command
TRIGGERMODE(4) = _trAUTO  'Rudders will move upon entering command
TRIGGERMODE(5) = _trAUTO  'Rudders will move upon entering command

'-------------------------------------------------------------------
'PROPELLER SETUP PARAMETERS
'Propeller acceleration rate.



'Scale each of the axes for drive/motor
SCALEFACTOR(0) = 14400      'AKD's set to 3,600 lines/rev or 14,400 quads/rev
SCALEFACTOR(1) = 14400      'Same as above
SCALEFACTOR(2) = 14400      'Same as above

'This should be changed after we get the motors tuned
FOLERRORMODE(1)=0
FOLERRORMODE(2)=0


'-------------------------------------------------------------------
' Set up Master Slave Relationship for the Servo(Propulsion) and Stepper
(Rudder) motors
```

```
'Propulsion Port servo motor (Axis 1)
MASTERSOURCE(0) = 4    'Master is axis velocity
 MASTERCHANNEL(1) = 0   'Slave axis 1 (Port Servo), Master axis is virtual
axis 0 (servo virtual axis)
 FOLLOWMODE(1) = 1      'Velocity locked mode
 FOLLOW(1) = -1.0        'Follow at 1:-1 ratio (Port Shaft turns counter
clockwise)
 GEARINGMODE(1) = 1

'Propulsion Starboard Servo Motor (Axis 2)
MASTERSOURCE(0) = 4    'Master is axis velocity
 MASTERCHANNEL(2) = 0   'Slave axis 2 (Starboard Servo), Master axis is
virtual axis 0 (servo virtual axis)
  FOLLOWMODE(2) = 1      'Velocity locked mode
  FOLLOW(2) = 1.0        'Follow at 1:1 ratio
  GEARINGMODE(2)= 1


'Rudder Port Stepper Motor (Axis 4)
MASTERSOURCE(0) = 0    'Master is axis position
  MASTERCHANNEL(4) = 3   'Slave axis 4 (Port Stepper), Master axis is virtual
axis 3 (stepper virtual axis)
  FOLLOWMODE(4) = 0      'Postion locked mode
  FOLLOW(4) = 1.0        'Follow at 1:1 ratio

'Rudder Starbaord Stepper Motor (Axis 5)
MASTERSOURCE(0) = 0    'Master is axis position
  MASTERCHANNEL(5) = 3   'Slave axis 5 (Starboard Stepper), Master axis is
virtual axis 3 (stepper virtual axis)
  FOLLOWMODE(5) = 0      'Position locked
  FOLLOW(5) = 1.0        'Follow at 1:1 ratio

'Defines Connection Status Identifier
'Define Link = CONNECT(11,241,1)


' Main program loop
Loop
' If Link = 0 Then ABORT Else Continue
End Loop


'event handler for changes in shaft speed
Event COMMS1
  JOG(ShaftMaster) = COMMS(ShaftSpeed)
End Event


'event handler for changes in rudder angle
Event COMMS2
  MOVEA(RudderMaster) = COMMS(RudderAngle)
End Event

Startup

  '--------------------------------
```

```
' Begin WorkBench Generated Startup Code
'--------------------------------

' Generated Monday, April 30, 2012
' for NextMove e100B Build 5622

Define ALL = 0, 1, 2, 3, 4, 5
Define DINBANKS = 0
Define DOUTBANKS = 0
Define ADCS = 0, 1
Define DACS = 0, 1, 2, 3
Define ENCODERS = 0, 1, 2

' Clear all motion
CANCELALL
Pause IDLE([ALL])
' Clear all errors
ERRORCLEAR(_egALL, -1)
Pause IDLE([ALL])
' Disable all axes
DRIVEENABLE([ALL]) = _false;

' Digital input configuration
INPUTMODE([DINBANKS]) = 0 ' 0x0
INPUTACTIVELEVEL([DINBANKS]) = 01111111111111111111 ' 0xfffff
INPUTPOSTRIGGER([DINBANKS]) = 0 ' 0x0
INPUTNEGTRIGGER([DINBANKS]) = 0 ' 0x0

' Analog input configuration
ADCMODE([ADCS]) = 0, 0

' Digital output configuration
GLOBALERROROUTPUT = -1
OUTPUTACTIVELEVEL([DOUTBANKS]) = 01111111111111 ' 0x1fff

' Analog output configuration
DACMODE([DACS]) = 0, 0, 0, 0

' Encoder configuration
ENCODERPRESCALE([ENCODERS]) = 1.00, 1.00, 1.00
ENCODERSCALE([ENCODERS]) = 14400.00, 14400.00, 1.00
ENCODERWRAP([ENCODERS]) = 0.00, 0.00, 0.00
ENCODERMODE([ENCODERS]) = 0, 0, 0

' --------------------------------
' Axis 0 configuration
' CONFIG(0) = _cfVirtual
' --------------------------------

' Axis 0 scaling
POSSCALEFACTOR(0) = 14400.00
VELSCALEFACTOR(0) = 14400.00
ACCELSCALEFACTOR(0) = 14400.00

' Axis 0 limits
SOFTLIMITMODE(0) = _emIGNORE
LIMITMODE(0) = _emCRASH_STOP_DISABLE
```

```
LIMITFORWARDINPUT(0) = -1
LIMITREVERSEINPUT(0) = -1
FOLERRORMODE(0) = _emCRASH_STOP_DISABLE
FOLERRORFATAL(0) = 0.07

' Axis 0 error modes
ERRORINPUT(0) = -1
ERRORINPUTMODE(0) = _emCRASH_STOP_DISABLE
ABORTMODE(0) = _emCRASH_STOP_DISABLE

' Axis 0 digital input events
STOPINPUT(0) = -1
STOPMODE(0) = _smDECEL
SUSPENDINPUT(0) = -1

' Axis 0 digital outputs
DRIVEENABLEOUTPUT(0) = -1

' Axis 0 gain terms
KPROP(0) = 0.00
KINT(0) = 0.00
KINTLIMIT(0) = 0.00
KINTMODE(0) = _itNEVER
KDERIV(0) = 0.00
KVEL(0) = 0.00
KVELFF(0) = 0.00
KACCEL(0) = 0.00

' Axis 0 profile parameters
PROFILEMODE(0) = _pmTRAPEZOIDAL
SPEED(0) = 0.00
ACCEL(0) = 4.00
DECEL(0) = 4.00
ERRORDECEL(0) = 20.83
ACCELJERK(0) = 208.33
DECELJERK(0) = 208.33
MOVEBUFFERSIZE(0) = 2

' Axis 0 homing parameters
HOMEINPUT(0) = -1
HOMESPEED(0) = 0.69
HOMEBACKOFF(0) = 10.00
HOMEACCEL(0) = 20.83
HOMEDECEL(0) = 20.83

' Axis 0 idle conditions
IDLEPOS(0) = 0.07
IDLEVEL(0) = 0.35
IDLETIME(0) = 0
IDLEMODE(0) = 0

' ---------------------------------
' Axis 1 configuration
' CONFIG(1) = _cfServo
' AXISPOSENCODER(1) = 0
' AXISVELENCODER(1) = 0
' AXISDAC(1) = 0
```

```
' --------------------------------

' Axis 1 scaling
POSSCALEFACTOR(1) = 14400.00
VELSCALEFACTOR(1) = 14400.00
ACCELSCALEFACTOR(1) = 14400.00

' Axis 1 limits
SOFTLIMITMODE(1) = _emIGNORE
LIMITMODE(1) = _emCRASH_STOP_DISABLE
LIMITFORWARDINPUT(1) = -1
LIMITREVERSEINPUT(1) = -1
FOLERRORMODE(1) = _emIGNORE
FOLERRORFATAL(1) = 0.07

' Axis 1 error modes
ERRORINPUT(1) = -1
ERRORINPUTMODE(1) = _emCRASH_STOP_DISABLE
ABORTMODE(1) = _emCRASH_STOP_DISABLE

' Axis 1 digital input events
STOPINPUT(1) = -1
STOPMODE(1) = _smDECEL
SUSPENDINPUT(1) = -1

' Axis 1 digital outputs
DRIVEENABLEOUTPUT(1) = 12

' Axis 1 gain terms
KPROP(1) = 0.05
KINT(1) = 0.50
KINTLIMIT(1) = 10.00
KINTMODE(1) = _itNEVER
KDERIV(1) = 7.50
KVEL(1) = 1.00
KVELFF(1) = 2.00
KACCEL(1) = 20.00

' Axis 1 profile parameters
PROFILEMODE(1) = _pmTRAPEZOIDAL
SPEED(1) = 0.00
ACCEL(1) = 4.00
DECEL(1) = 4.00
ERRORDECEL(1) = 20.83
ACCELJERK(1) = 208.33
DECELJERK(1) = 208.33
MOVEBUFFERSIZE(1) = 2

' Axis 1 homing parameters
HOMEINPUT(1) = -1
HOMESPEED(1) = 0.69
HOMEBACKOFF(1) = 10.00
HOMEACCEL(1) = 20.83
HOMEDECEL(1) = 20.83

' Axis 1 idle conditions
IDLEPOS(1) = 0.07
```

```
IDLEVEL(1) = 0.35
IDLETIME(1) = 0
IDLEMODE(1) = 0

' --------------------------------
' Axis 2 configuration
' CONFIG(2) = _cfServo
' AXISPOSENCODER(2) = 1
' AXISVELENCODER(2) = 1
' AXISDAC(2) = 1
' --------------------------------

' Axis 2 scaling
POSSCALEFACTOR(2) = 14400.00
VELSCALEFACTOR(2) = 14400.00
ACCELSCALEFACTOR(2) = 14400.00

' Axis 2 limits
SOFTLIMITMODE(2) = _emIGNORE
LIMITMODE(2) = _emCRASH_STOP_DISABLE
LIMITFORWARDINPUT(2) = -1
LIMITREVERSEINPUT(2) = -1
FOLERRORMODE(2) = _emIGNORE
FOLERRORFATAL(2) = 0.07

' Axis 2 error modes
ERRORINPUT(2) = -1
ERRORINPUTMODE(2) = _emCRASH_STOP_DISABLE
ABORTMODE(2) = _emCRASH_STOP_DISABLE

' Axis 2 digital input events
STOPINPUT(2) = -1
STOPMODE(2) = _smDECEL
SUSPENDINPUT(2) = -1

' Axis 2 digital outputs
DRIVEENABLEOUTPUT(2) = 12

' Axis 2 gain terms
KPROP(2) = 0.05
KINT(2) = 0.50
KINTLIMIT(2) = 10.00
KINTMODE(2) = _itNEVER
KDERIV(2) = 7.50
KVEL(2) = 1.00
KVELFF(2) = 2.00
KACCEL(2) = 20.00

' Axis 2 profile parameters
PROFILEMODE(2) = _pmTRAPEZOIDAL
SPEED(2) = 0.00
ACCEL(2) = 4.00
DECEL(2) = 4.00
ERRORDECEL(2) = 20.83
ACCELJERK(2) = 208.33
DECELJERK(2) = 208.33
MOVEBUFFERSIZE(2) = 2
```

```
' Axis 2 homing parameters
HOMEINPUT(2) = -1
HOMESPEED(2) = 0.69
HOMEBACKOFF(2) = 10.00
HOMEACCEL(2) = 20.83
HOMEDECEL(2) = 20.83

' Axis 2 idle conditions
IDLEPOS(2) = 0.07
IDLEVEL(2) = 0.35
IDLETIME(2) = 0
IDLEMODE(2) = 0

' --------------------------------
' Axis 3 configuration
' CONFIG(3) = _cfVirtual
' --------------------------------

' Axis 3 scaling
POSSCALEFACTOR(3) = 100.00
VELSCALEFACTOR(3) = 100.00
ACCELSCALEFACTOR(3) = 100.00

' Axis 3 limits
SOFTLIMITMODE(3) = _emCALL_HANDLER
SOFTLIMITFORWARD(3) = 36.00
SOFTLIMITREVERSE(3) = -36.00
LIMITMODE(3) = _emCRASH_STOP_DISABLE
LIMITFORWARDINPUT(3) = -1
LIMITREVERSEINPUT(3) = -1
FOLERRORMODE(3) = _emCRASH_STOP_DISABLE
FOLERRORFATAL(3) = 10.00

' Axis 3 error modes
ERRORINPUT(3) = -1
ERRORINPUTMODE(3) = _emCRASH_STOP_DISABLE
ABORTMODE(3) = _emCRASH_STOP_DISABLE

' Axis 3 digital input events
STOPINPUT(3) = -1
STOPMODE(3) = _smDECEL
SUSPENDINPUT(3) = -1

' Axis 3 digital outputs
DRIVEENABLEOUTPUT(3) = -1

' Axis 3 gain terms
KPROP(3) = 0.00
KINT(3) = 0.00
KINTLIMIT(3) = 0.00
KINTMODE(3) = _itNEVER
KDERIV(3) = 0.00
KVEL(3) = 0.00
KVELFF(3) = 0.00
KACCEL(3) = 0.00
```

```
' Axis 3 profile parameters
PROFILEMODE(3) = _pmTRAPEZOIDAL
SPEED(3) = 98.60
ACCEL(3) = 3000.00
DECEL(3) = 3000.00
ERRORDECEL(3) = 3000.00
ACCELJERK(3) = 30000.00
DECELJERK(3) = 30000.00
MOVEBUFFERSIZE(3) = 2

' Axis 3 homing parameters
HOMEINPUT(3) = -1
HOMESPEED(3) = 100.00
HOMEBACKOFF(3) = 10.00
HOMEACCEL(3) = 3000.00
HOMEDECEL(3) = 3000.00

' Axis 3 idle conditions
IDLEPOS(3) = 10.00
IDLEVEL(3) = 50.00
IDLETIME(3) = 0
IDLEMODE(3) = 0

' --------------------------------
' Axis 4 configuration
' CONFIG(4) = _cfStepper
' AXISPDOUTPUT(4) = 0
' --------------------------------

' Axis 4 scaling
POSSCALEFACTOR(4) = 100.00
VELSCALEFACTOR(4) = 100.00
ACCELSCALEFACTOR(4) = 100.00

' Axis 4 limits
SOFTLIMITMODE(4) = _emIGNORE
LIMITMODE(4) = _emCRASH_STOP_DISABLE
LIMITFORWARDINPUT(4) = -1
LIMITREVERSEINPUT(4) = -1

' Axis 4 error modes
ERRORINPUT(4) = -1
ERRORINPUTMODE(4) = _emCRASH_STOP_DISABLE
ABORTMODE(4) = _emCRASH_STOP_DISABLE

' Axis 4 digital input events
STOPINPUT(4) = -1
STOPMODE(4) = _smDECEL
SUSPENDINPUT(4) = -1

' Axis 4 digital outputs
DRIVEENABLEOUTPUT(4) = -1

' Axis 4 profile parameters
PROFILEMODE(4) = _pmTRAPEZOIDAL
SPEED(4) = 400.00
ACCEL(4) = 3000.00
```

```
DECEL(4) = 3000.00
ERRORDECEL(4) = 3000.00
ACCELJERK(4) = 30000.00
DECELJERK(4) = 30000.00
MOVEBUFFERSIZE(4) = 2

' Axis 4 homing parameters
HOMEINPUT(4) = -1
HOMESPEED(4) = 100.00
HOMEBACKOFF(4) = 10.00
HOMEACCEL(4) = 3000.00
HOMEDECEL(4) = 3000.00

' Axis 4 idle conditions
IDLEPOS(4) = 10.00
IDLEVEL(4) = 50.00
IDLETIME(4) = 0
IDLEMODE(4) = 0

' --------------------------------
' Axis 5 configuration
' CONFIG(5) = _cfStepper
' AXISPDOUTPUT(5) = 1
' --------------------------------

' Axis 5 scaling
POSSCALEFACTOR(5) = 100.00
VELSCALEFACTOR(5) = 100.00
ACCELSCALEFACTOR(5) = 100.00

' Axis 5 limits
SOFTLIMITMODE(5) = _emIGNORE
LIMITMODE(5) = _emCRASH_STOP_DISABLE
LIMITFORWARDINPUT(5) = -1
LIMITREVERSEINPUT(5) = -1

' Axis 5 error modes
ERRORINPUT(5) = -1
ERRORINPUTMODE(5) = _emCRASH_STOP_DISABLE
ABORTMODE(5) = _emCRASH_STOP_DISABLE

' Axis 5 digital input events
STOPINPUT(5) = -1
STOPMODE(5) = _smDECEL
SUSPENDINPUT(5) = -1

' Axis 5 digital outputs
DRIVEENABLEOUTPUT(5) = -1

' Axis 5 profile parameters
PROFILEMODE(5) = _pmTRAPEZOIDAL
SPEED(5) = 400.00
ACCEL(5) = 3000.00
DECEL(5) = 3000.00
ERRORDECEL(5) = 3000.00
ACCELJERK(5) = 30000.00
DECELJERK(5) = 30000.00
```

```
  MOVEBUFFERSIZE(5) = 2

  ' Axis 5 homing parameters
  HOMEINPUT(5) = -1
  HOMESPEED(5) = 100.00
  HOMEBACKOFF(5) = 10.00
  HOMEACCEL(5) = 3000.00
  HOMEDECEL(5) = 3000.00

  ' Axis 5 idle conditions
  IDLEPOS(5) = 10.00
  IDLEVEL(5) = 50.00
  IDLETIME(5) = 0
  IDLEMODE(5) = 0

  ' Terminal configuration
  TERMINALMODE(_TERM1) = 01
  TERMINALMODE(_TERM2) = 01
  TERMINALMODE(_TERM3) = 01
  TERMINALMODE(_TERM4) = 01
  TERMINALMODE(_TERM5) = 01

  '--------------------------------
  ' End WorkBench Generated Startup Code
  '--------------------------------

  ' Add user startup code here...

End Startup
```

Appendix E-Ship Construction Specification to Maritime Applied Physics

Massachusetts Institute of Technology

October 24, 2011

Paul Dillingham
Maritime Applied Physics Corporation
1850 Frankfurst Ave.
Baltimore, MD
21226

Change 1

1. Motor Mount dimensions
2. Rudder Fairing dimensions

1. Purpose

The purpose of this document is to outline the contract specifications for the construction of a 1/30th scale model of the DTMB 5415 hull for Professor Chryssostomos Chryssostomidis, director of MIT Sea Grant. The CAD drawings shown are solely to provide guidance to the contractor and not all components on the CAD drawing are the responsibility of the contractor. The contractor is responsible for construction of the hull, window, platform bulkheads, platforms, motor mount, shaft fairing, shaft strut, shaft, and rudder fairing. The contractor is responsible for meeting the specifications outlined below, as listed in order from bow to stern. Any questions or design alteration suggestions should be forwarded to LT David Cope (copedm@mit.edu).

2. Background

The hull form will be a free-running, remote-controlled hydrodynamic imagining and testing platform. It will be utilized in large maneuvering basins and/or open water. The windows along the hull will provide viewports so that various imaging technologies can be used to visualize the flow around the hull.

3. Ship Specification

a. General – The tolerance for all measurements is ± 0.1 inch unless stated otherwise.

b. Hull form - The hull will be modeled after the DTMB 5415 hull form, scaled to 1/30th of the original design. The hull shall be made of a suitable foam core, either machined or carved, and encased in sufficient layers of fiberglass. The hull must have enough structural support to carry its design load of 675 lbs. The sheer line of the hull will be extended such that it is horizontal to the baseline and at the same elevation as the bow, 21.3 inches above baseline (BL), to prevent swamping (shown in Scaled5415.igs). It will be painted standard model yellow. Draft marks will be painted on both the bow and the stern in 0.5 inch increments from 6 inches to 10 inches from the baseline. The CAD files, represent the external limits of the hull shell. The principal dimensions of the scaled model are listed below.

i. Length Overall (LOA) - 201.5 inches
ii. Design Waterline (DWL) - 186.7 inches
iii. Draft (T) - 8.07 inches
iv. Beam at the Waterline (BWL) - 25.0 inches

MIT Sea Grant
Building E38-300
77 Massachusetts Avenue
Cambridge, Massachusetts
02139-4307
Phone 617-253-7041
Fax 617-258-5730
Seagrant.mit.edu

v. Displacement - 692.0 pounds
vi. Station Spacing – 9.32 inches
vii. Number of stations - 21
viii. Forward Perpendicular (FP) – 13.25 inches aft of the bow

c. Hull window - The window will be built into the hull and conform to the original shape of the hull. It will be no thicker than 0.5 inch and have no seams. The window will extend no less than 2.0 inches above the DWL. The fore and aft extents of the window are listed below and measured from the FP. Add 13.25 inches to measure from the bow.

i. Stern Window
1. 165.8 inches (Fwd extent)
2. Transom

d. Hull Bulkheads – The hull will have three (3) platforms built in to accommodate the internal machinery and payload. Each will consist of a series of bulkheads that span the breadth of the hull and allow for a plate structure to be placed on top to secure equipment. The bulkheads should be no wider than 1.0 inch. The fore extents, aft extents and heights from the baseline are listed below. The extents are measured from the FP. Add 13.25 inches to measure from the bow.

i. Platform 1 (Fwd)
1. Station 5, 46.6 inches (Fwd Extent)
2. 104.7 inches (Aft Extent)
3. 3.0 inches (Height from Baseline)

ii. Platform 2 (Aft)-This platform cannot obstruct the shaft lines, as shown in the CAD model. The walls of the bulkhead cannot extend beyond 5.5 inches from the centerline.
1. Station 14, 130.5 inches (Fwd Extent)
2. Station 17, 158.4 inches (Aft Extent)
3. 5.5 inches (Height from Baseline)

iii. Platform 3 (Stern)- This platform supports the turning gear that will consist of two stepper motors mounted vertically. It should have enough depth and strength to tap holes for mounting of the motors.
1. 178 inches (Fwd Extent)
2. Transom (Aft Extent)
3. 14.2 inches (Height of top from Baseline)

e. Propulsion Motor Mount – This is a solid platform that can be tapped to mount the two propulsion motors.
1. 106.0 inches (Fwd Extent)
2. 122.0 inches (Aft Extent)
3. 2.0 inches (Height from Baseline)

f. Hull Platforms – The platforms will fit over the bulkheads and be used to secure the internal machinery and equipment. They will conform to the sides of the hull and must be easily removable from the bulkheads so that ballast may be added between the bulkheads. Machinable aluminum is the preferable material and the depth will be at least 1/8".

g. Shaft Fairing – The shaft fairings will be cylindrical in shape with a filleted end and extend no greater than 147.0 inches aft of the FP. It will have sufficient shaft seals and radial bearings for continuous operation of 1,000 rpm. It will be at an angle of 2.95 degrees from the baseline and the shaft will exit the fairing at

i. 147.0 inches aft of the FP
ii. 6.1 inches off the centerline
iii. 2.6 inches above the baseline

h. Shaft Strut – The shaft struts will be cylindrical in shape with the forward end filleted. The legs of the struts will have a NACA 0012 foil shape and have sufficient strength to house the shafting.

i. 173.7 inches aft of the FP (origin of aft opening, where the forward part of the propeller hub will meet, center of cylinder)
ii. Length of approximately 2.9 inches

i. Shaft – MAPC's proposed shaft design will be utilized, and it will meet the requirements listed in the following paragraph. The propeller shafts will be 1.0 inch in diameter, 45.0 inches in length and made of stainless steel. They will be positioned such that the propeller end of the shaft is 174.7 inches aft of the FP. The end attaching to the propeller will be machined to 5/16 inch in diameter for 2.0 inches from the end and be threaded with 5/16"-24 size thread. Additionally, a 3/16 inch hole will be drilled perpendicular to and centered through the shaft on the same end as the threads, with its center located 1.85 inches from the edge. On the end of the shaft in the boat, the shaft will be machined to a diameter of 0.5 inches for 1.0 inch from the end, and have a standard 1/8" (Wd.) x 1/16" (Dp.) ANSI keyway to be fitted to a flexible coupling as shown below. A separate CAD drawing of the shaft is provided. Note that the threads on the propeller end are not shown in the drawing.

j. Rudder Fairing & Foundation – The rudder fairings will be of a NACA 0018 foil shape and have the extents listed below. The top will be faired into the hull and the bottom surface will be parallel to the baseline. The fairing will be drilled through after delivery and a rudder shaft will be installed. Therefore the fairing must be made of an easily bored but equally strong material.
i. Leading edge - 179.9 inches aft of FP
ii. Trailing edge - 185.4 inches aft of FP
iii. Chord Length – 5.5 inches
iv. Chord line offset from centerline – 5.5 inches
v. Height of lower edge to baseline – 6 inches
vi. Height of upper edge (internal to hull) to baseline - 8.4 inches

Sincerely,

David Cope
LT USN

Appendix F-Internal Equipment General Arrangement

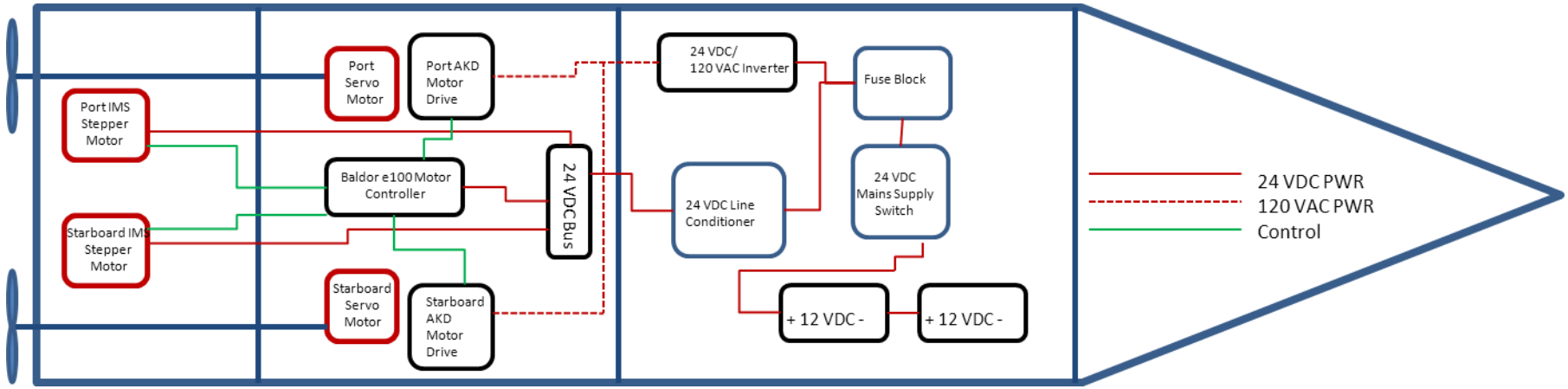

Appendix G-Model Controller and Motor Wiring

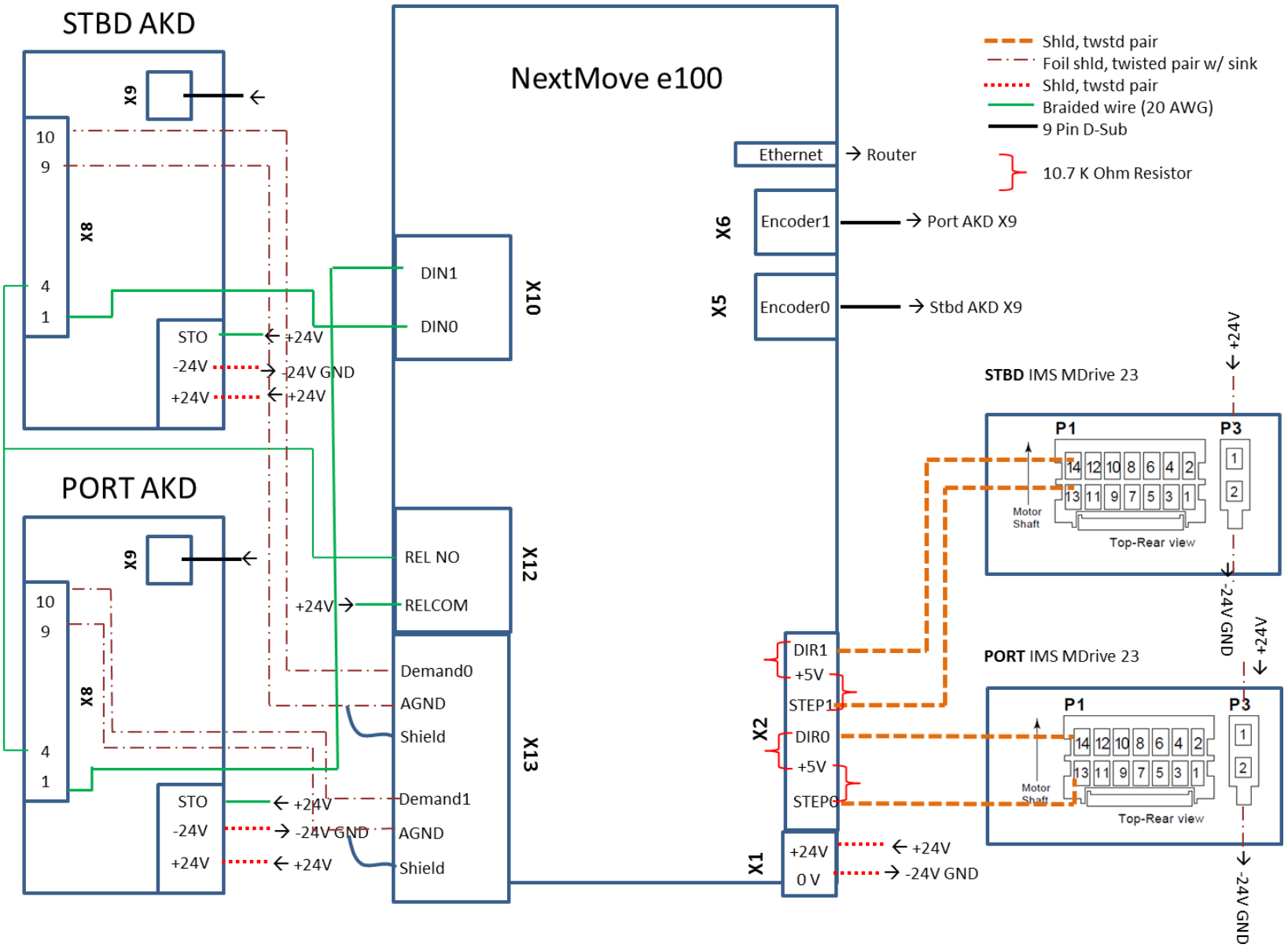

Appendix H-Model Weight Report

COMPONENT	WT (lbs)	VCG (ft abv base)	Vert Moment	LCG (ft aft bow)	Long Moment
HULL STRUCTURE					
Hull-Fwd Port	79.52	0.76	60.44	6.17	490.64
Hull-Fwd Stbd	79.52	0.77	61.23	6.12	486.66
Aft Port	56.28	0.79	44.46	12.81	720.95
Aft Stbd	56.28	0.80	45.02	12.83	722.07
Bow	17.60	0.13	2.29	1.98	34.85
Fore Deck	24.29	1.69	41.05	2.74	66.55
Mid Deck	44.55	1.68	74.84	9.70	432.14
Aft Deck	11.56	1.68	19.42	15.56	179.87
Fore Mounting Plate	8.67	0.25	2.17	7.44	64.50
Mid Mounting Plate	7.82	0.45	3.52	12.68	99.16
Aft Mounting Plate	5.31	1.16	6.16	15.52	82.41
Window	4.00	0.60	2.40	15.67	62.68
PROPULSION					
AKM Motor Port	5.38	0.36	1.94	11.00	59.18
AKM Motor Starboard	5.38	0.36	1.94	11.00	59.18
Motor Drive Port	2.20		0.00		0.00
Motor Drive Starboard	2.20		0.00		0.00
Propeller Port	0.39		0.00		0.00
Propeller Starboard	0.39		0.00		0.00
Flex coupling Starboard	0.51				
Flex coupling Port	0.51				
Shaft Port	3.11	-0.22	-0.68	13.40	41.67
Shaft Starboard	3.11	-0.22	-0.68	13.40	41.67
Shaft Housing Starboard	1.60	-0.22	-0.35	13.37	21.39
Shaft Housing Port	1.60	-0.22	-0.35	13.37	21.39
Shaft Fairing Port	0.29	-0.20	-0.06	13.00	3.77
Shaft Fairing Starboard	0.29	-0.20	-0.06	13.00	3.77
Port Strut Assem	0.52	-0.33	-0.17	15.45	8.03
Starboard Strut Assem	0.52	-0.33	-0.17	15.45	8.03
AKM Motor Mount Port	3.87		0.00	11.00	42.56
AKM Motor Mount Starboard	3.87		0.00	11.00	42.56
MANEUVERING					
Rudder & Post Port	1.33		0.00	16.30	21.70
Rudder & Post Starboard	1.33		0.00	16.30	21.70
Stepper Motor Port	2.56		0.00	16.30	41.73
Stepper Motor Starboard	2.56		0.00	16.30	41.73
Rudder Fairing Port	0.46	0.56	0.26	16.30	7.50
Rudder Fairing Starboard	0.46	0.56	0.26	16.30	7.50
Rudder Shaft Housing Port	0.17	0.88	0.15	16.30	2.77
Rudder Shaft Housing Starboard	0.17	0.88	0.15	16.30	2.77
Rudder Platform	3.63	1.18	4.28	16.30	59.17
COMUNICATIONS & DATA					
Wireless Router-EnGenius 9850	0.44		0.00		0.00
Wireless Antenna	0.85		0.00		0.00
Baldor Motor Controller	1.87		0.00		0.00
					0.00
MISCELLANEOUS					
24 VDC Line Conditioner	0.94		0.00		0.00
12VDC to 120 VAC Inverter	16.18		0.00		0.00
Battery 1	57.00	0.53	30.21		0.00
Battery 2	57.00	0.53	30.21		0.00
					0.00
BALLAST					

WT Total (lbs)	VCG(ft)	LCG(ft)	Total Long Moment	Total Vertical Moment
578.07	0.74	6.92	4002.26	429.86

Full Scale			1/30th Scale Design		Model Actual		Diff
VCG	24.78	ft	0.83	ft	0.74	ft	-
LCB	269.26	ft aft bow	8.98	ft aft bow	8.98		-
LCG	-	-	-	-	6.92	ft	-
LCG-LCB	-	-	-	-	-2.05	ft	-
Disp	8350.00	LT	692.74	lbs	578.07	lbs	-114.67

Appendix I-Bill of Materials

	Budget						Expenditure							Subtotal
Group	Component	Manufacturer	Model	Qty	$/Unit	$ Total	Component	Manufacturer/Supplier	Model	Received?	Qty	$/Unit	$ Total	Difference
Structure	Hull Structure	MAPC		1	47,676.69	47,676.69	Hull & Window	MAPC	-	Received	1.00	53,385.36	53,385.36	
	Propeller	MIT 3D Print		2	2,000.00	4,000.00	Rudder Material	Advanced Autoparts	-	Received	1.00	20.77	20.77	
	Rudder	MIT 3D Print		2	1,000.00	2,000.00	Right Prop/end caps Print	Edgerton	-	Received	1.00	102.00	102.00	
	Window	MAPC		1	5,708.67	5,708.67	Left Prop Print	Edgerton	-	Received	1.00	100.00	100.00	
							Rudder Posts	MIT Central	-	Received	1.00	200.00	200.00	
							Rudder Assembly	MAPC	-	Received	1.00	1,922.91	1,922.91	
							Rudder-Print	Edgerton	-	Received	1.00	70.00	70.00	
							Propeller Nickel Plate	RePliForm	-	Received	1.00	616.00	616.00	
							Model Lid	MAPC	-	Received	1.00	818.70	818.70	
					Subtotal	59,385.36						Subtotal	56,417.04	2,968.32
Propulsion	Motor	Koll Morgen	AKM42E	2	800.00	1,600.00	Motors and Drives	Target Electric	Multiple	Received	1.00	4,883.11	4,883.11	
	Motor Drive	Koll Morgen	AKD-B01206	2	600.00	1,200.00	Boat Electrical Hardware	West Marine	-	Received	1.00	267.90	267.90	
	Controller	Galil	DMC-1415	2	595.00	1,190.00	Motor Controller	Baldor/Target Electric	NEX100-08SB	Received	1.00	2,420.00	2,420.00	
	Controller Software	Galil	Galil Tools	1	0.00	0.00								
Maneuvering	Stepper Motor	IMS		2	800.00	1,600.00								
	Motor Controller	IMS		2	500.00	1,000.00								
					Subtotal	6,590.00						Subtotal	7,571.01	-981.01
Communication/Data	Wireless Access Point	Netgear	WG602	1	56.99	56.99	Wireless Hardware	Newegg	Multiple	Received	1.00	238.35	238.35	
	Wireless Router	Netgear	WGR614	1	33.99	33.99	CAT 5 Crossover Cables	Show Me Cables	590-07 RD	Received	5.00	4.20	21.00	
	Wireless Antenna	Netgear	ANT2409-20000S	1	99.00	99.00	Microcontroller+GPS	Sparkfun	-	Received	1.00	151.10	151.10	
	GPS/GPS Shield	SparkFun	RTL-10709	1	79.95	79.95	Antenna converter cables	L-com	-	Received	1.00	69.95	69.95	
	MicroController	Arduino	Mega 2560	1	58.95	58.95								
	Arduino Project Enclosure	Sparkfun	PRT-10088	1	11.95	11.95								
	Wall Adapter Power Supply 9VDC 650mA (for Micro Controller)	SparkFun	TOL-00298	1	5.95	5.95								
	9DOF Sensor Stick	SparkFun	SEN-10724	1	99.50	99.50								
					Subtotal	446.28						Subtotal	480.40	-34.12
Misc & Support Equip	Hardware	MMC		1	251.77	251.77	Casters	McMaster	EzRoll Swivel	Received	6.00	33.38	200.28	
	12VDC to 120 VAC Inverter	AIMS	PWRI200012S	1	500.00	500.00	Misc Hardware	Home Depot	-	Received	1.00	44.34	44.34	
	Battery	Interstate	SC31DM	6	45.00	270.00	Misc Hardware	McMaster	-	Received	1.00	1,067.34	1,067.34	
	Trailer	TraileX	SUT-200-S	1	914.00	914.00	AC to DC converter (24V)	McMaster	7009K18	Received	1.00	146.83	146.83	
							Inverter	AIMS	PWRI200012S	Received	1.00	499.00	499.00	
							Batteries	Sears	27M Die Hard DC	Received	1.00	403.68	403.68	
							24 VDC Line Cond	Imtra	Intervolt	Received	1.00	246.10	246.10	
							Lifting Straps	McMaster	8937T442	Received	1.00	156.00	156.00	
							Inverter	Star Marine Depot	Xantrex Prosine 1800	Received	1.00	1,376.69	1,376.69	
							Misc Hardware	McMaster	Multiple	Received	1.00	53.17	53.17	
							Misc Hardware	McMaster	Multiple	Received	1.00	126.17	126.17	
					Subtotal	1,935.77						Subtotal	4,319.60	-2,383.83
							Expenditures not Budgeted							
Additional Funding Opportunites not Budgeted	Custom Trailer/Cradle			1	1,000.00	1,000.00	IMU	Microstrain	3DM GX3-45	Received	1.00	3,795.00	3,795.00	
	Vortex Rollers			1	1,000.00	1,000.00								
	Azimuthing Pod/Hull Modification			1	4,000.00	4,000.00								
	Resistor Bank			1	1,000.00	1,000.00								
	Accelerometer			1	2,000.00	2,000.00								
	Dedicated Laptop			1	2,000.00	2,000.00								
	SAPIV Setup			1	15,000.00	15,000.00								
	Nickel plating propellers			1	1,000.00	1,000.00								
				Additional Funding		27,000.00						Subtotal	3,795.00	
				Total Baseline		68,357.41				Total Expenditure to Date			68,788.05	-430.64
				Total_w/Additional		95,357.41				Total Proposed Expenditure			72,583.05	